The Value of In-Reservoir Energy Storage for Flexible Dispatch of Geothermal Power*

Wilson Ricks[a], Jack Norbeck[b], Jesse Jenkins[a]

[a]*Princeton University, 86 Olden St., Princeton, 08540, New Jersey, USA*
[b]*Fervo Energy, 708 Main St., Houston, 77002, Texas, USA*

Abstract

Geothermal systems making use of advanced drilling and well stimulation techniques have the potential to provide tens to hundreds of gigawatts of clean electricity generation in the United States by 2050. With near-zero variable costs, geothermal plants have traditionally been envisioned as providing "baseload" power, generating at their maximum rated output at all times. However, as variable renewable energy sources (VREs) see greater deployment in energy markets, baseload power is becoming increasingly less competitive relative to flexible, dispatchable generation and energy storage. Herein we conduct an analysis of the potential for future geothermal plants to provide both of these services, taking advantage of the natural properties of confined, engineered geothermal reservoirs to store energy in the form of accumulated, pressurized geofluid and provide flexible load-following generation. We develop a linear optimization model based on multi-physics reservoir simulations that captures the transient pressure and flow behaviors within a confined, engineered geothermal reservoir. We then optimize the investment decisions and hourly operations of a power plant exploiting such a reservoir against a set of historical and modeled future electricity price series. We find that operational flexibility and in-reservoir energy storage can significantly enhance the value of geothermal plants in markets with high VRE penetration, with energy value improvements of up to 60% relative to conventional baseload plants operating under identical conditions. Across a range of real-

*This is a preprint. Read the final paper at:
Ricks, W., Norbeck, J. and Jenkins, J. "The Value of In-Reservoir Energy Storage for Flexible Dispatch of Geothermal Power." *Applied Energy*, 313 (2022), 118807, https://doi.org/10.1016/j.apenergy.2022.118807

istic subsurface and operational conditions, our modeling demonstrates that confined, engineered geothermal reservoirs can provide large and effectively free energy storage capacity, with round-trip storage efficiencies comparable to those of leading grid-scale energy storage technologies. Optimized operational strategies indicate that flexible geothermal plants can provide both short- and long-duration energy storage, prioritizing output during periods of high electricity prices. Sensitivity analysis assesses the variation in outcomes across a range of subsurface conditions and cost scenarios.

1. Introduction

Firm, low-carbon resources have been identified as critical for cost-effective deep decarbonization of electricity systems [1, 2]. Geothermal power is one such resource, with added benefits of full renewability and minimal land and resource use relative to other sources of electricity [3]. Despite these advantages, geothermal deployment has historically been constrained to a very select set of sites where naturally-occurring hydrothermal reservoirs can be exploited for electricity generation. Due in large part to this lack of resource availability, geothermal power currently supplies only 0.4% of annual electricity demand in the United States [4], with a total installed generating capacity of under 4 GW [5].

Through technology innovation, drilling cost reductions, and improved exploration techniques, it may be possible to significantly increase the economically viable resource base for geothermal energy. For example, studies by the USGS have indicated that up to 30 GW of undiscovered hydrothermal resources may exist in the US [6, 7], which could be identified using novel geophysical exploration techniques. In addition, recent innovations in horizontal drilling, reservoir stimulation techniques, and other Enhanced Geothermal System (EGS) technologies can enable geothermal development in formations that would otherwise be unsuitable or uneconomic [8]. Relatively shallow EGS resources underlie much of the western United States, and successful development of this technology could unlock hundreds to thousands of gigawatts of geothermal resource potential nationwide, with up to 120 GW deployable by 2050 [7, 9, 10].

Still, the economic outlook for geothermal power is unclear in a rapidly evolving electricity market. Geothermal plants typically operate as "baseload" power, generating at their maximum rated capacity at all times [11]. This

has historically been a viable operating strategy, but shifting electricity market conditions are eroding the economic value of baseload power relative to more flexible alternatives. As electricity systems move toward complete decarbonization, it is generally accepted that variable renewable energy (VRE) sources will supply an increasingly significant share of total generation [12, 13, 14]. However, increased VRE penetration in electricity markets drives greater volatility in net load and electricity prices [15], can lead to overgeneration [12], and has been associated with negative pricing episodes of increased length and severity [16]. Under such conditions, greater system flexibility is needed in order to maintain supply-demand balance in the grid, limiting the system value inflexible baseload resources [17, 18, 19, 20, 21, 22, 23, 24]. From an economic perspective, fast-ramping generators with low fixed costs, which can save money by only generating when electricity prices are high, and energy storage devices that shift generation to valuable periods, can have a competitive advantage over baseload generators in a grid with significant VRE penetration [2].

1.1. Flexibility in Existing Geothermal Plants

To improve the future economic viability of geothermal power, next-generation geothermal power plants must be designed with flexibility in mind. From a surface facilities perspective, most geothermal power plants are already capable of operating with a high degree of flexibility, which is achieved by altering geothermal fluid production rate or production fluid enthalpy. Surface generator designed with flexibility in mind, particularly binary-cycle plants, can ramp efficiently between 10% and 100% output at rates of up to 30% nominal power per minute [25]. Some binary plants today take advantage of this high degree of flexibility to provide ancillary services to the grid [11], but the economic benefits are limited because reducing production does not reduce operating costs for such plants. In general, the high fixed costs and near-zero variable costs of geothermal power plants strongly disincentivize deviation from a baseload operating strategy.

One strategy by which geothermal plants can derive benefits from flexibility is to ramp down production during periods of negative electricity prices, thereby avoiding losses. Millstein et al. [26] optimized geothermal plant operations against historical real-time electricity price series and found that existing binary-cycle plants in the U.S. could improve their energy value (measured as the average price of electricity per unit geothermal generation) by an average of 5.5% by operating in this manner. While not insignificant,

these improvements are ultimately the result of cutting losses during negative pricing episodes, and this mode of operation does nothing to increase the value of the geothermal plant outside of those periods.

There is some evidence that flash steam geothermal plants, which rely on reservoir pressure rather than pumping to drive production flow, may be able to derive additional benefits from flexibility outside of avoiding negative prices. In an analysis of curtailment events at the Geysers geothermal field, Goyal [27] found that multi-week reductions in steam production were routinely followed by short-term increases in production flow, driven by increased reservoir pressure. This behavior could in theory be exploited to "shift" plant generation from times with lower electricity prices to times with higher prices. However, flash steam plants are generally more limited in their ability to curtail production than binary plants [26], and it should be noted that the "puff" events observed by Goyal [27] only recovered roughly 15% of curtailed generation due to pressure leakoff in the reservoir. Analysis by Millstein et al. [26] indicates that the benefits of flexibility for a plant with these characteristics would be less than those for a fully-curtailable binary plant that could not induce periods of flush production.

1.2. Geothermal Energy Storage

While conventional, stand-alone geothermal plants are therefore limited in their ability to extract additional value from flexible operations, a range of concepts have been proposed for improving plant value by using a geothermal reservoir as a medium for thermal or geomechanical energy storage. Thermal energy storage can be enabled by coupling a geothermal plant with another high-temperature thermal energy source such as a solar thermal or nuclear power plant. Thermal energy from the coupled plant can be used during times of energy overabundance to heat the geothermal reservoir, allowing for greater energy production at later times [28, 29]. This hybrid approach is promising, but depends on the mutual cost-effectiveness and co-location potential of multiple generating technologies. It cannot improve the performance of a stand-alone geothermal plant with no outside source of thermal energy. Another thermal energy storage concept is CO_2 plume geothermal, which charges and discharges by moving a CO_2 working fluid between two isolated subsurface reservoirs at different temperatures [30]. The reliance of this latter concept on unique geologic conditions likely limits its potential for large-scale adoption.

Geomechanical geothermal energy storage has been explored in the context of sedimentary basin CO_2 sequestration, particularly by Buscheck et al. [31]. In the CO_2-Bulk Energy Storage (CO_2-BES) concept, concentric rings of CO_2 and brine injection and production wells create hydraulically confined regions where injected fluid can be efficiently recovered rather than being lost to leakoff. By injecting fluid and reducing production during times of energy overabundance, such systems can build up pressure and accumulate working fluid in the reservoir. Increased pressure can then be used to drive artesian production flow during periods of energy scarcity, effectively providing grid-scale energy storage. Ogland-Hand et al. [32] found that such systems could theoretically provide efficient energy storage for durations of up to a week.

Although there may be value in CO_2-BES energy storage in the context of CO_2 sequestration operations, sedimentary basins tend to be poorly suited for stand-alone geothermal power production. The vast majority of high-heat (and therefore economically attractive) geothermal resources in the United States exist elsewhere, particularly in low-permeability settings where EGS would be the most viable extraction method [10]. Though EGS plants operate under subsurface conditions that differ greatly from those in sedimentary basins, they may actually be well-suited to providing a form of geomechanical energy storage similar to that proposed by Buscheck et al. [31]. In typical EGS designs, the low-permeability rock matrix surrounding an engineered geothermal reservoir can provide natural hydraulic confinement without the need for complex well configurations. This behavior was demonstrated by the engineered reservoir at Fenton Hill, a Department of Energy EGS test site. At this site, fractures created during a stimulation treatment program provided high-conductivity flow paths between an injection well and production well, and the relatively low-permeability formation surrounding the fractures prevented fluid leakoff, causing confined reservoir behavior [33]. Periodic reductions in production flow rate with no changes to injection rate were shown to result in increased reservoir pressure, which was effectively retained over many hours due to the confined nature of the reservoir. When the production wellhead backpressure was subsequently reduced, the accumulated reservoir pressure drove production flow at a higher rate than the standard injection rate for a period of several hours.

The results of the Fenton Hill EGS project demonstrated the potential for *in-reservoir energy storage* (IRES) in such systems, wherein accumulated geofluid and reservoir pressure are used to shift the output of a geothermal plant from one time to another. Importantly, the ability to store energy in

this manner is an inherent property of an EGS reservoir requiring no additional capital expenditure. Given the critical importance of EGS to large-scale geothermal deployment [10], and the value of both flexible generation and energy storage in electricity systems [34, 35, 36], the ability for EGS to provide both these services has the potential to significantly increase the value and deployment potential of geothermal power as a whole.

1.3. Contribution of this Work

Successful deployment of flexible EGS power with IRES will depend on 1) developing a broader understanding of the subsurface characteristics that promote effective energy storage, and 2) developing innovative operational strategies that maximize the economic benefit of operating flexibly. To address these issues, we first use a numerical geothermal reservoir model to evaluate the technical feasibility of a flexible geothermal operational strategy in a synthetic system similar to the Fenton Hill EGS test site. We then employ plant-level optimization modeling to assess the impact of flexible operations and IRES on the economic value of a single next-generation geothermal power plant. We develop a linear optimization model capturing the transient pressure and flow behavior within a geothermal reservoir system designed for flexible operations, and use this model to co-optimize plant investments and operations against both historical and modeled future electricity price series. We further characterize the optimal operating modes of a flexible geothermal power plant and assess the sensitivity of model outputs to variations in critical uncertain parameters. The goal of this work is to quantify the economic value that can be derived from flexible operations and IRES for geothermal power plants, and to identify primary areas of focus for ongoing research and development of this technology.

2. Methods

2.1. Representative Plant Design.

EGS is an emerging technology, and most proposed plans for its commercialization hinge on using early "near-field" projects to accelerate technological learning [10]. These projects would target the hot but low-permeability formations surrounding known hydrothermal sites, where minimal exploration and drilling is necessary for development. Sufficient cost reductions in these early phases could enable the economical development of "deep EGS"

resources, those at depths of 3 km or more located in low-permeability basement rock [37]. It is this deep resource that represents the vast majority of geothermal potential worldwide [10]. In this paper we focus on the transitional point in this approach, considering an EGS plant mining a 218 °C low-permeability geothermal resource at a depth of 3 km. We use this representative case to analyze the impact of flexibility and energy storage on the economics of early EGS projects.

In our analysis we consider a triplet well design similar to those discussed in Gringarten et al. [38], Olson et al. [39], Li et al. [40], and others. An injection well is drilled to the target depth and deviated to produce a 1.5 km horizontal section. Hydraulic stimulation is used to create regularly-spaced vertical fractures along this interval, and two production wells are drilled in parallel and at opposite orientation to the injection well, intersecting these fractures and creating a long horizontal reservoir. The vertical fractures serve as flow pathways that create a strong hydraulic connection between the injection and production wellbores, as well as the reservoir contact area, to enable sustained heat recovery over the system life. The configuration assessed in this paper is designed to produce 10.1 MW of electric power per well triplet. This well completion and reservoir engineering design is illustrated in Fig. 1. The rock matrix surrounding the engineered reservoir is assumed to have low but non-zero permeability, representative of the hot, low-permeability formations that make up the majority of developable EGS resources worldwide. Recognizing the significant locational variation in subsurface characteristics across potential EGS sites worldwide, as well as uncertainties in technology costs and performance, we include a set of sensitivity cases covering the likely ranges of these parameters.

In the configuration described above, reservoir pressure alone is used to drive artesian geofluid flow in the production wells. Produced fluid is run through a binary-cycle surface plant before being re-injected into the reservoir. The use of a binary-cycle surface plant allows for highly-flexible generation with no additional operational and maintenance costs [11].

2.2. Modeling Approach.

We employ a bottom-up approach to modeling the performance of a flexible geothermal plant, using multi-physics numerical reservoir simulations to develop a linear optimization model, which is used to evaluate the economics of flexible operations. Reservoir simulations are done using a commercial

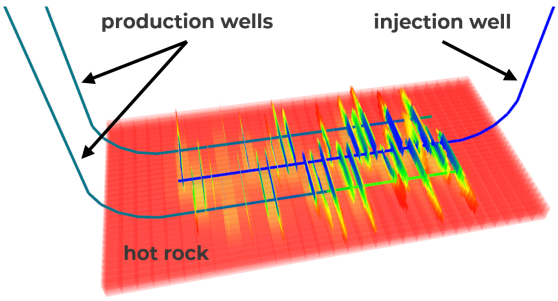

Figure 1: Three-dimensional model of the triplet well system, wherein two production wells are drilled at opposite orientation to a single horizontal injection well. The wells are connected hydraulically by a series of evenly-spaced vertical fractures that provide the primary flow paths. The fractures are able to deform mechanically in response to changes in pressure and stress, providing fluid storage volume in the subsurface.

geothermal reservoir simulation software package that includes detailed calculations of wellbore friction, fracture deformation and pressure response, fluid leakoff, and heat transfer [41, 42]. These simulations provide all of the information necessary for evaluation of reservoir performance under different operating conditions and strategies.

To allow for techno-economic optimization of plant investments and operations, we develop a secondary linear optimization model based on the numerical reservoir simulation results. We simulate the transient pressure response at the injection and production well bottom-holes to stepwise changes in injection and production rates. Piecewise linearization and subsequent linear superposition of this pressure response function allow us to capture the transient reservoir pressure response to variable pumping rates within a linear programming (LP) framework. The LP model also considers the dependence of production rate on reservoir pressure and variable "parasitic" load due to injection pumping. The reservoir simulation and optimization modeling methodology is described in further detail in Appendix A. Fig. 2 illustrates the tight agreement between the simplified LP model and the multi-physics simulation results.

2.3. Techno-Economic Optimization.

The LP model introduced in Section 2.2 captures the effects of changes to production and injection rates at hourly timesteps. These two flow rates are the model's operational decision variables. Reductions to production rate

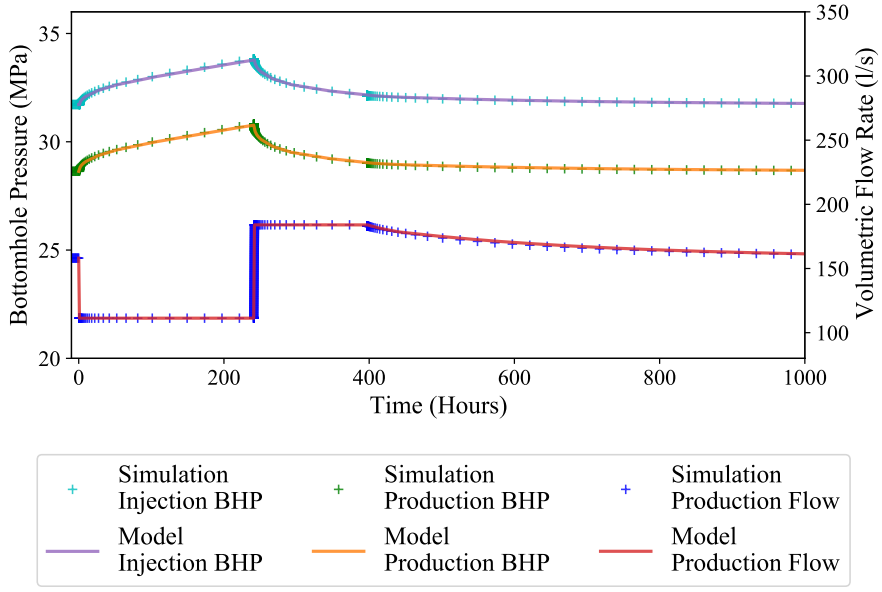

Figure 2: The LP optimization model and the numerical reservoir simulation executing an identical sequence of operational decisions. Injection rate is held constant, while production flow is partially shut in for a period of 240 hours, causing the injection and production well bottomhole pressures to rise. The production well is subsequently opened to allow up to a specified maximum flow rate, and both pressures and flow decline back to their steady-state values. Simulation results are shown as point data, while model results are shown as continuous data.

(or increases to injection) lead to increased reservoir pressure. The production well bottomhole pressure (BHP) determines the maximum achievable production flow rate at each model timestep. The maximum usable production flow rate is further constrained by the generating capacity of the surface plant, and the size of the plant's grid interconnection. It is assumed for the purposes of this work that the binary organic Rankine cycle (ORC) surface plant can handle geofluid flow rates up to 10% above its design point with minimal loss of efficiency and without any additional capital expenditure [43]. Beyond this point, the surface facilities must be oversized (with respect to a plant designed for constant flow from the same reservoir) to take advantage of increased production flow. Surface plant and grid interconnection oversizing are included as investment decisions, and are penalized in the objective function to reflect increased construction, maintenance and insurance costs. Injection pumps may also be oversized at a specified cost in order to accommodate greater injection pressures and flow rates. Financial assumptions for surface facilities oversizing are outlined in Appendix B.6. Costs used in the baseline model are presented in Table 1, along with baseline values for other important model parameters. Due to the very high flexibility of ORC units, the model does not impose any hourly ramping or minimum generation constraints.

Table 1: Parameter values for the base case model

Parameter	Symbol	Value
Surface plant capital cost	C_{plant}	\$2050/kW$_{net}$
Interconnection capital cost	C_{IC}	\$130/kW
Injection pump capital cost	C_{pump}	\$400/kW
Reservoir temperature	T_{res}	218 C
Production temperature	T_{prod}	210 C
Injection temperature	T_{inj}	70 C
Maximum increase to reservoir pressure	ΔP_{max}	3.5 MPa
Number of reservoir fractures	N_f	100
Fracture conductivity	K_f	4.5×10^{-12} m^3
Matrix permeability	k_m	9.9×10^{-19} m^2
Matrix porosity	ϕ_m	0.05

The optimization model takes an hourly electricity price series as input, and co-optimizes investment and hourly operational decisions to maximize plant revenue over a single weather year. Only investment costs corresponding to surface facilities oversizing are modeled, and all costs associated with

the reservoir, well field, and conventional surface facilities are considered sunk. Though the wellfield and subsurface reservoir at a given plant could theoretically be engineered to maximize the value of the facility when operating flexibly, such an optimization is beyond the scope of the current work. Our model thus assesses only the relative costs and benefits associated with flexibility and energy storage at a plant otherwise designed for baseload operations.

It should be noted that this work is not intended to predict true revenues for geothermal power plants, which are often determined by long-term power purchase agreements, renewable energy credits, capacity payments, and other factors. Rather, we use wholesale electricity prices as a means to measure the market value of generation at each hour, and evaluate the overall improvement in a geothermal plant's energy value that can be derived from flexible operations and energy storage. This approach is designed to assess geothermal's overall appeal to potential power offtakers, which will be determined in large part by the value of geothermal energy in wholesale electricity markets. The use of a fixed electricity price series in this work assumes that the flexible geothermal plant in question operates as a price-taker, i.e. that it does not have enough market power to influence the price of electricity through its operational decisions. This is a good approximation of the conditions that would be experienced by the first flexible EGS plants to enter a regional electricity market.

In this paper we optimize flexible geothermal investments and operations against eight historical and eight modeled future electricity price series. The historical series consist of real-time locational marginal price data for the year 2019 taken from seven grid nodes in the Western Interconnection and one in the Texas Interconnection, sourced from the CAISO OASIS tool [44] and ERCOT's online market prices database [45], respectively. The nodes in the Western Interconnection are located in states and regions with identified geothermal resources, and are intended to represent a diversity of possible electricity market conditions that might be encountered by an early flexible geothermal plant. The node from Texas is not located in an area with significant geothermal potential but is instead selected to represent an electricity market with high wind power penetration.

In addition to these historical price series, we also consider synthetic national price series for the year 2030 created using the GenX electricity system optimization model [46]. We consider 2030 as a target year for full commercial deployment of flexible EGS, and create eight price series for this year

in GenX to reflect different potential market scenarios. These include a set of four series assuming various technology deployment and load scenarios but no policy changes, and an additional four considering the same scenarios under a national $60/ton carbon tax. Each set of four includes one baseline scenario, which represents the results of a simple capacity expansion optimization with no changes to base system inputs. The second scenario uses an alternate load profile peaking in winter, which is more representative of northeastern states under increased electrification. The third and fourth scenarios alter wind and solar input parameters to prioritize deployment of one of these resources over the other. Though these modeled price series are spatially unresolved, and do not capture the same level of volatility seen in real electricity markets, they allow us to evaluate the performance of flexible geothermal in systems with significantly higher VRE penetration than exists in most markets today. For example, the "high solar" and "high wind" carbon tax scenarios each see VREs making up just under 50% of installed generating capacity nationwide.

3. Results and Discussion

3.1. Base Case Results.

Optimization results under baseline reservoir performance and plant costing assumptions for historical price series are given in Table 2, and results for modeled 2030 price series are given in Table 3. All energy value and component-sizing results are presented with respect to the corresponding values for a baseload geothermal plant. The average hourly energy value per MW of net generating capacity for such a plant is equal to the average hourly price of electricity for each series. Relative improvement over this "baseload" average energy value from a curtailment-only operating strategy similar to that discussed in Millstein et al. [26] is given for both sets of price series. This number represents the degree to which value could be improved if the plant curtailed generation during negative pricing episodes but did not store the lost energy. Value improvement from full flexibility represents the average energy value of the same plant under flexible operations with IRES, after subtracting the annuitized cost of any oversizing of surface facilities. For all flexible cases, energy value is given with respect to the total annual generation of a baseload plant. This allows for meaningful comparison of results in cases where annual flexible generation is less than baseload (e.g. due to increased pumping loads). The optimal degree of plant, interconnection,

and injection pump oversizing for a fully flexible plant is given with respect to the sizes of these components in an inflexible baseload plant.

Results for historical price series indicate that flexible operation and energy storage produce greater energy value than baseload operation in all cases, with a minimum relative value improvement of 6% and a maximum of 44%. The greatest level of improvement occurs at the southern California node, which represents an electricity market with the highest level of solar penetration in the United States [4]. Significant improvement is also observed at the Arizona and Nevada nodes, as well as at the wind-heavy Texas node. In these markets, high VRE penetration drives greater electricity price variability, increasing flexible geothermal's relative advantage over baseload by providing more opportunities for arbitrage via energy storage. Conversely, benefits from flexibility and energy storage are greatly reduced in locations with more stable electricity prices. The northern California node, for example, is located near The Geysers geothermal installation, where a steady supply of baseload power leads to relatively stable electricity prices and reduces benefits from flexibility. Though simple curtailment can occasionally provide appreciable value improvements, improvements from full flexibility are much larger in all cases, even taking into account the extra costs associated with surface facilities oversizing.

Results for modeled future price series indicate similar trends to those observed for historical price series. Flexibility and energy storage offer greater relative benefits in a market with a large carbon tax, which results in greater VRE deployment and higher marginal prices during periods of low VRE output. In cases without a carbon tax, energy value improvements are relatively consistent across the baseline, high solar and high wind cases. The high-VRE cases see a much larger relative improvement over the baseline when a carbon tax is also in place. With and without a carbon tax, value improvements are greater for the high wind case than for the high solar case. The "winter peaking" case sees very reduced benefits under both policy scenarios, but this case is also not very representative of areas in the US with significant geothermal potential [10]. Because the modeled price series used in this paper reflect a perfectly planned and operated system with minimal volatility and low geospatial resolution, the relative benefits of flexibility in similar real-life systems are likely to be greater than those reported here.

Analysis of the 16 historical and modeled future price series (see Appendix D.1) shows that the level of energy value improvement from flexible operations and energy storage cannot be easily deduced analytically. For

some price series, very high peak prices appear to be the primary source of value. This is the case for the Texas historical price series, which features a very high price cap of $9000/MWh. For others, frequent negative pricing rewards energy storage. In general, the number of hours of the year for which prices are at or below $0/MWh appears to be a good, but imperfect indicator of the level of benefit that can be extracted from full flexibility. Zero or negative prices allow flexible geothermal plants to boost injection rates without regard for increased parasitic loads, increasing generating capacity during subsequent periods of positive pricing.

Across all price series, optimal surface plant oversizing (e.g. construction of additional surface plant gross generating capacity beyond that of a baseload plant) ranges from 0-61% of baseload surface plant gross capacity. The greatest levels of oversizing are observed for the historical Texas series and the future carbon tax scenarios. For the Texas series, oversizing allows for increased generation during short periods of extremely high prices. In the future carbon tax scenarios, it is likely that higher average electricity prices decrease the cost of plant oversizing relative to the benefits that can be extracted. Interconnection oversizing (e.g. construction of greater transmission interconnection capacity than baseload surface plant net generating capacity) is fairly significant and consistent across all price series, due to very low capital costs relative to other components. Even if the gross surface plant capacity itself is not expanded, oversizing the interconnection allows the geothermal facility to deliver more net power at certain times by reducing parasitic load from pumping. Pump oversizing, which is required for operation at higher injection rates and BHPs, shows significant variation between price series. It is most extreme for series with many hours of zero or negative pricing, which allow the plant to temporarily boost its pumping rate without incurring an economic penalty. Given the variance in optimal component sizing across different electricity market conditions, geothermal developers should make efforts to forecast the evolution of a local electricity market over a flexible plant's operational lifetime before beginning surface facilities construction. Doing so will minimize the risk of suboptimal plant and interconnection sizing. It is possible that in the case of an undersized plant, extra "peaking" turbines, interconnection reinforcements, or supplementary pumps could be added later in its lifetime to enable greater flexibility.

Table 2: Energy value and optimal investment results for historical price series in the base case model.

Node Location	Baseload Energy Value ($/MWh Avg.)	Value Improvement: Curtailment Only (% of Baseload)	Value Improvement: Full Flexibility (% of Baseload)	Plant Oversizing (% of Baseload Plant Capacity)	Interconnection Oversizing (% of Baseload IC Capacity)	Pump Oversizing (% of Baseload Pump Capacity)
AZ	31.3	5	20	23	48	129
N-CA	34.8	0	9	5	26	62
S-CA	25.9	19	44	16	40	636
ID	29.6	0	8	0	21	42
NV	30.5	6	18	8	31	95
OR	27.3	0	6	0	20	37
TX	34.6	0	22	61	93	85
UT	27.8	2	10	0	21	45

Table 3: Energy value and optimal investment results for modeled future price series in the base case model.

Scenario	Baseload Energy Value ($/MWh Avg.)	Value Improvement: Curtailment Only (% of Baseload)	Value Improvement: Full Flexibility (% of Baseload)	Plant Oversizing (% of Baseload Plant Capacity)	Interconnection Oversizing (% of Baseload IC Capacity)	Pump Oversizing (% of Baseload Pump Capacity)
BAU Baseline	29.6	2	14	6	25	61
BAU Winter Peak	29.4	0	3	0	18	18
BAU High Solar	28.9	0	11	4	24	46
BAU High Wind	32.2	1	15	13	35	77
CO_2 Tax Baseline	49.3	0	15	20	45	148
CO_2 Tax Winter Peak	51.1	0	11	8	29	82
CO_2 Tax High Solar	46.6	0	24	33	60	189
CO_2 Tax High Wind	46.5	0	26	29	55	203

3.2. Optimal Operational Strategies.

Analysis of the operational decisions made by the optimization model in response to specific price structures provides insight into the sources of value for fully flexible geothermal power. Fig. 3 presents pressure and flow behaviors during a selected period of 200 hours, for the base case model run against the southern California historical price series, as well as hourly electricity prices during the same period. As expected, the model tends to reduce production rate and increase injection rate during periods of low electricity prices, which causes reservoir pressure to rise. When prices are high, the model will reduce injection while boosting production to the maximum level allowed by the capacity of the surface facilities. This process occurs on a diurnal basis, following the daily peaks and troughs in electricity prices, but also occurs over much longer timescales. For the 200 hour period referenced in Fig. 3, electricity prices are generally higher in the second set of 100 hours than in the first. The model responds to this price structure by injecting more and producing less over the first 100 hour period, causing the reservoir pressure to become elevated over this entire period. During the second period, this accumulated pressure allows the plant to maintain its maximum production while reducing injection, thereby limiting parasitic load and maximizing net generation. This behavior demonstrates that with the right subsurface conditions, fully flexible geothermal is capable of providing long-duration energy storage over periods of hundreds of hours. This is possible because a large amount of geofluid can be stored within the reservoir before the maximum allowed pressure is reached. The energy storage capacity of a flexible geothermal reservoir is discussed further in Section 3.4.

Figs. 4 and 5 show behaviors in response to price series with different characteristics. Fig. 4 illustrates the optimal operating strategy in response to the historical Texas price series, which features mostly low, stable prices punctuated by extreme price spikes. In this case, the model builds extra generating capacity to take advantage of these spikes, and organizes all operations around maximizing net generation during these periods. Fig. 5 illustrates behavior for a section of the 2030 carbon-tax high-wind price series featuring a long period of near-zero prices followed by intermittent but fairly stable periods of high prices. The plant curtails generation completely during the low-price period, allowing it to maintain maximum generation for more than 20 hours during the high-price periods. The facility takes advantage of short intervals of near-zero prices to quickly "recharge" the reservoir, allowing it to maintain high net generation.

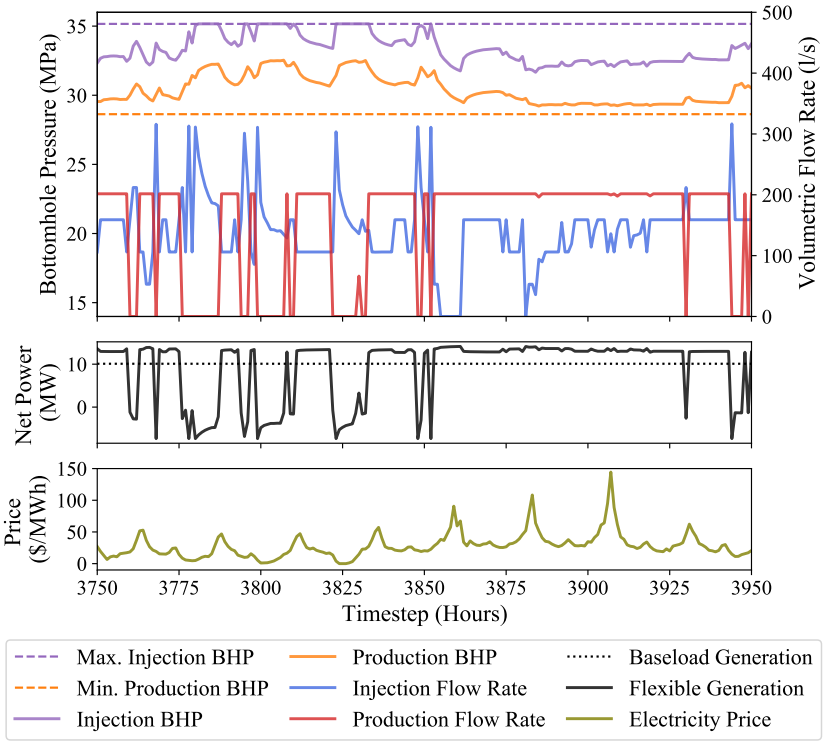

Figure 3: Optimal flexible operational strategy during a selected period of 200 hours for the southern California historical price series in the base case model. The upper plot gives injection and production well BHPs and injection and production flow rates at hourly timesteps during this period. The middle plot gives net generation under both baseload and flexible operating strategies, and lower plot gives hourly electricity prices. Model timestep 1 corresponds to 00:00 on January 1.

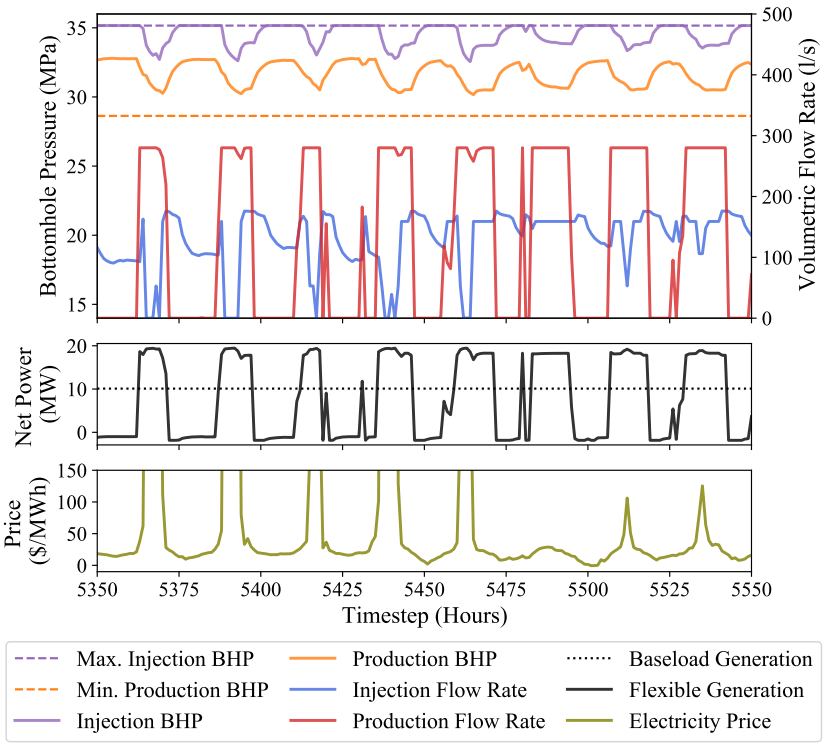

Figure 4: Same as Fig. 3, for the Texas historical price series.

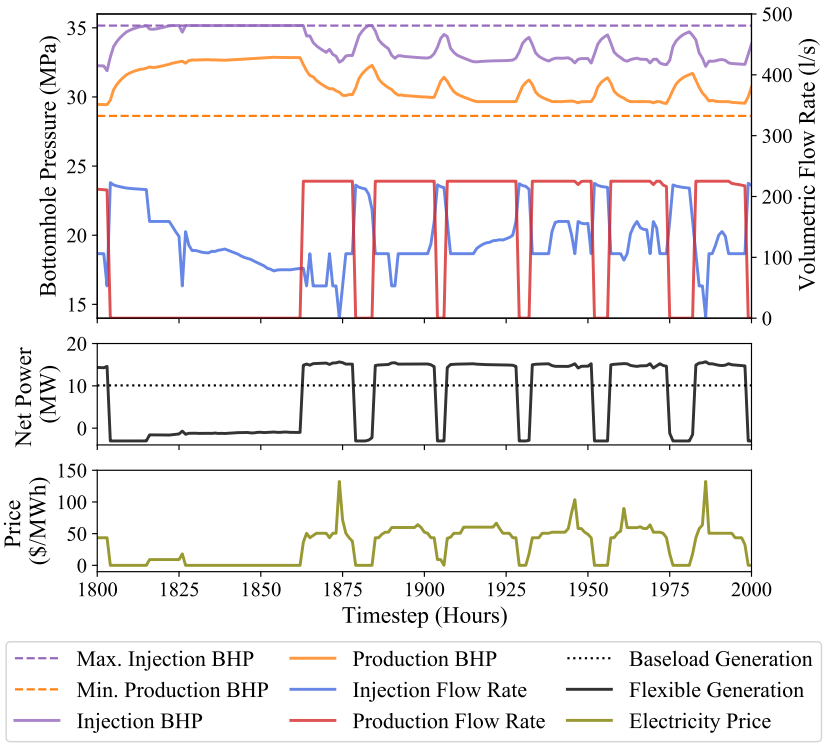

Figure 5: Same as Fig. 3, for the 2030 CO_2 tax high wind price series.

3.3. Sensitivity Analysis.

In addition to the base case, we also investigate 15 sensitivity cases designed to cover the range of parametric variation that might occur across different geologic, regulatory, and technology advancement scenarios. Individual sensitivity cases adjust a single parameter value relative to the base case, allowing us to evaluate the sensitivity of the results outlined in Section 3.1 to variations in each of these parameters. Sensitivity parameters include the cost of surface plant oversizing C_{plant}, the effect of flexible operations on surface facilities maintenance costs OM_s, the maximum allowable pressure increase in the reservoir ΔP_{max}, fracture conductivity K_f, number of fractures N_f, and rock matrix permeability k_m. We include high and low bounding cases for all parameters except OM_s, as well as mid-high and mid-low cases for both K_f and k_m. Assuming that flexible operations would only increase maintenance costs, we include only a high bounding case for the OM_s parameter. The parameter variations associated with each sensitivity case are outlined in Table 4. Fig. 6 shows the variation in total annual energy output for a baseload geothermal plant across all sensitivity cases. Flexible operations and investments are optimized for each sensitivity case against all 16 historical and modeled future electricity price series. Fig. 7 presents the relative improvement in energy value from full flexibility for each of the 240 total cases analyzed.

Results indicate that a reduction in surface plant cost generally improves the value of flexible operations, especially for price series with a high level of optimal plant oversizing. Reduced plant cost allows for greater surface oversizing, which in turn enables greater generation during peak-price periods. Increasing surface plant cost has the opposite effect, though often to a lesser extent.

It is possible that frequent cycling of generators and injection pumps under flexible operation could increase the maintenance costs of these facilities. These additional costs would affect the entire facility, not just the oversized portion. Lew et al. [47] found that increased cycling in response to greater VRE penetration raised the O&M costs per MWh of fossil-fueled thermal power plants by 2-5%. Here, we find that a 10% increase in maintenance costs for both the ORC power plant and injection pump under operational flexibility reduces the relative value of IRES only marginally. Given the high flexibility of ORC units relative to conventional thermal generators, it is likely that true surface OM penalties from IRES will be well below this threshold.

ΔP_{max} limits the allowable pressure increase within the reservoir, and effectively represents the maximum "charge capacity" of the system. Anticipating that excessive reservoir pressurization could produce deleterious effects, including induced seismicity [48], we limit ΔP_{max} to 3.5 MPa in the base case model. We find that increasing this value by 1.5 MPa does not produce major benefits in any scenario. Reducing ΔP_{max} by the same amount limits the benefits of flexibility in only a small number of cases. Overall, it seems that the 3.5 MPa pressurization limit used in this paper unlocks nearly all of the benefits of flexibility, and that a 2 MPa limit still captures most of these benefits. The seismic risk associated with this level of pressurization should be further characterized through field testing.

We find that reduced matrix permeability has the most significant effect on flexible operations, cutting relative benefits by up to a third in the lowest-permeability case. Reduced matrix permeability limits the migration of geofluid between the fractures and the matrix, leading to more significant pressure changes in response to pumping. This increased pressure response causes the reservoir to reach its pressure cap more quickly, effectively reducing the energy storage capacity of the system. Increased matrix permeability leads to greater baseload energy production, due to greater natural flow rates from the reservoir, but does not appreciably improve the relative benefits of flexible operation over baseload. These results suggest that it will be necessary to fully characterize the subsurface properties of a potential geothermal site in order to accurately assess the local potential for flexible operation and IRES.

Changes to the fracture conductivity K_f have a significant effect on baseload energy output, as fracture conductivity is the primary factor determining parasitic power requirements for injection pumping. While reduced fracture conductivity reduces the energy output of a baseload plant by increasing parasitic load from injection, it increases the relative benefits of flexibility. The opposite is true for cases with increased fracture conductivity, which see greater baseload energy output but reduced relative benefits from flexibility. This occurs because shifting injection pumping to times with lower electricity prices has a greater relative impact in scenarios where injection load consumes a greater proportion of net plant generation. Flexible operations can thus reduce the negative impact of lower-than-desired fracture conductivity on the economics of a geothermal plant.

Increasing or reducing the number of fractures present in the engineered reservoir has several effects. A smaller number of fractures will reduce the

overall transmissivity of the reservoir, leading to higher parasitic load from injection pumping. It will also reduce the surface area over which the fracture system interacts with the rock matrix, somewhat limiting the exchange of fluid and therefor increasing the pressure response to pumping. We find that reducing the number of fractures reduces baseload energy output somewhat, and that increasing the number of fractures does the opposite. The effect on relative benefits of flexibility over baseload operations is unpredictable, but is generally fairly small. Overall, results are fairly insensitive to changes in the number of fractures. A larger number of fractures will therefore be desirable, as this will increase the heat extraction efficiency of the system with minimal negative effects.

Table 4: Sensitivity case names and parametric variations

Scenario	Description
C^-_{plant}	Surface plant capital cost reduced by 33%.
C^+_{plant}	Surface plant capital cost increased by 50%.
OM^+_s	Surface maintenance costs increased by 10% when operating flexibly.
ΔP^-_{max}	Maximum allowable reservoir pressure reduced by 1.5 MPa.
ΔP^+_{max}	Maximum allowable reservoir pressure increased by 1.5 MPa.
k^{--}_m	Matrix permeability reduced to 1/100 of base case value.
k^-_m	Matrix permeability reduced to 1/10 of base case value.
k^+_m	Matrix permeability increased to 10x base case value.
k^{++}_m	Matrix permeability increased to 100x base case value.
K^{--}_f	Fracture conductivity reduced to 1.1×10^{-12} m^3.
K^-_f	Fracture conductivity reduced to 2.3×10^{-12} m^3.
K^+_f	Fracture conductivity increased to 1.2×10^{-11} m^3.
K^{++}_f	Fracture conductivity increased to 3.2×10^{-11} m^3.
N^-_f	Number of fractures reduced to 50.
N^+_f	Number of fractures increased to 150.

3.4. Energy Storage Efficiency and Capacity.

A fully flexible geothermal power plant can be thought of as an energy storage device stacked on top of an inflexible baseload generator. If the plant is at zero "state of charge," it will produce a constant amount of power equal to its baseload capacity. Negative deviation from this steady-state output, either through increased injection load or curtailed production, can be thought of as equivalent to "charging" the geothermal energy storage.

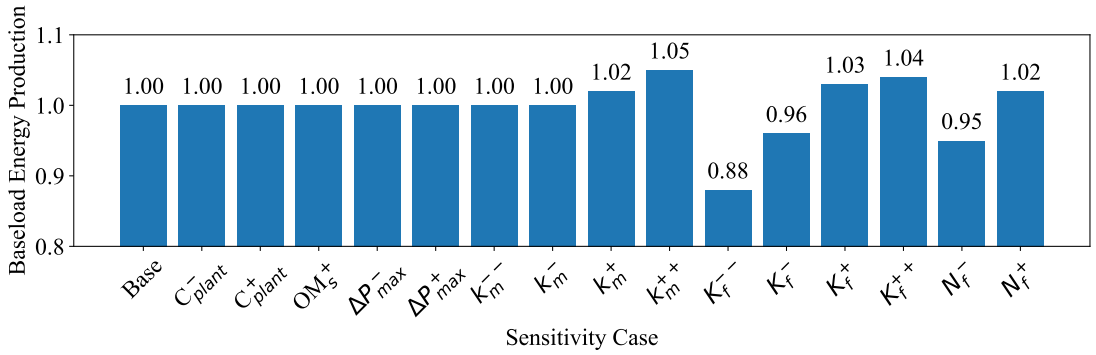

Figure 6: Annual energy production for a baseload geothermal plant in each sensitivity case, normalized with respect to the energy production of a base-case plant.

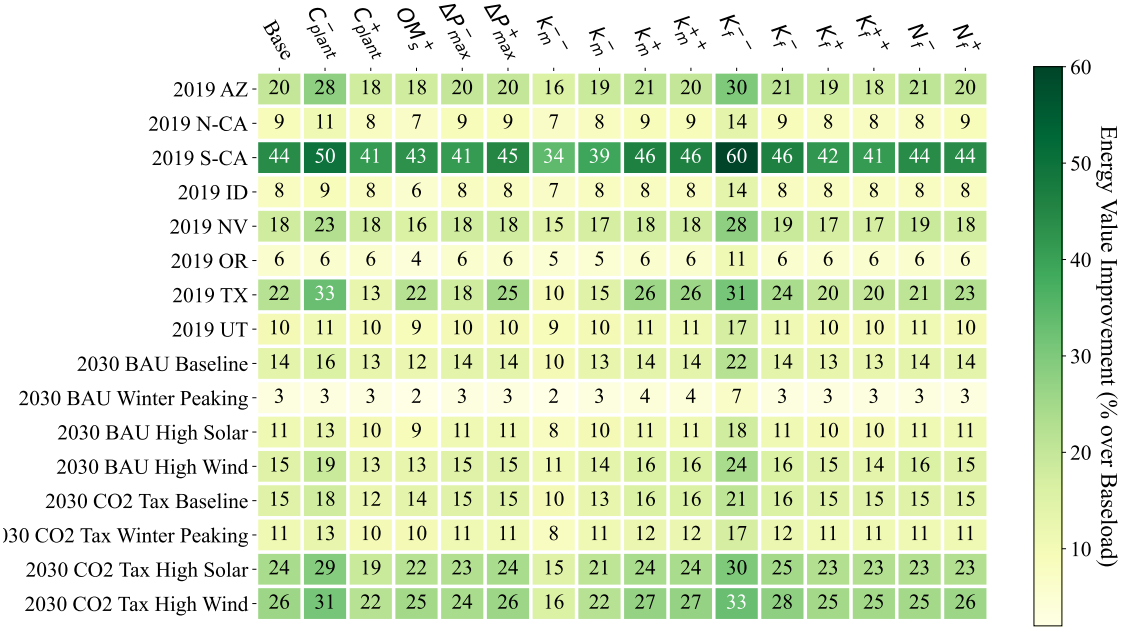

Figure 7: Relative energy value improvement over baseload for a fully flexible geothermal plant across 16 sensitivity cases and 16 electricity price series.

From the perspective of the electricity grid, a reduction in generation from the geothermal plant appears identical to an increased load from energy storage charging at the same location. Likewise, positive deviation from the plant's baseload generation represents discharging of the geothermal energy storage. Based on these interpretations, the average round-trip efficiency of flexible geothermal energy storage over a year of operations can be calculated via the following equation:

$$\eta_{avg} = \left| \frac{\sum_{t \in [1:8760]} \Delta G_t^+}{\sum_{t \in [1:8760]} \Delta G_t^-} \right|, \tag{1}$$

where $\Delta G_t^{\pm}$ is the deviation of net plant generation at hour t from the steady-state baseload output, either positive or negative. Round-trip efficiency is calculated for each of the 240 cases analyzed in this paper. These results are given in Fig. D.15. Optimal efficiency is variable across price series and sensitivity cases, but is typically in excess of 80%. This value is comparable to the round-trip efficiencies of both pumped-hydro energy storage and lithium-ion batteries, two leading grid-scale energy storage technologies [49]. As a general rule, flexible geothermal plants with energy storage have lower annual generation than their baseload counterparts. Despite this, the fact that the flexible plants prioritize generation at times of high electricity prices significantly improves the overall value of their energy relative to baseload plants. Notably, analysis of model results indicates that only a small portion of the reduced net generation from flexible operations is attributable to reduced *gross* generation. Instead, the vast majority of "round trip losses" occur due to increases in parasitic load from injection pumping during flexible operation. This extra pumping power is a consequence of maintaining the reservoir at an elevated pressure, but also of increasing injection rate above its steady-state level during certain periods. Injection pumping power increases approximately quadratically with injection rate, meaning that there is a tradeoff between faster "charging" and overall storage efficiency. The observed variation in optimal efficiency can be attributed to the model ignoring or even encouraging losses during periods of very low or negative electricity prices, while instead prioritizing fast charging using cheap energy.

In addition to price series analysis, we conduct a set of controlled tests using the same optimization model to quantify the total energy storage capacity of IRES. To optimize energy capacity, we provide the model with an artificial input price series featuring near-zero positive prices for a period of

240 hours, followed by an extended period of extremely high prices. Plant investment costs are not taken into consideration, and both maximum injection and production flow rates are capped at 4/3 the corresponding steady-state flow rates for a baseload plant. The model's objective is therefore to store as much energy as possible in the 240 hour "charging period" so that it can maximize the total net generation during the subsequent "discharging period." The results of this experiment can be used to set an upper bound on the energy storage capacity of a flexible geothermal plant. Fig. 8 shows behavior of the base case model operating in this controlled scenario. Energy storage capacity is calculated as the deviation from baseload generation integrated over the entire discharge period, and is normalized with respect to the net generating capacity of the baseload surface plant (ignoring injection pumping load), which scales in size with the subsurface reservoir. Fig. 9 shows the maximum energy storage capacity per MW of net baseload plant capacity for each sensitivity case.

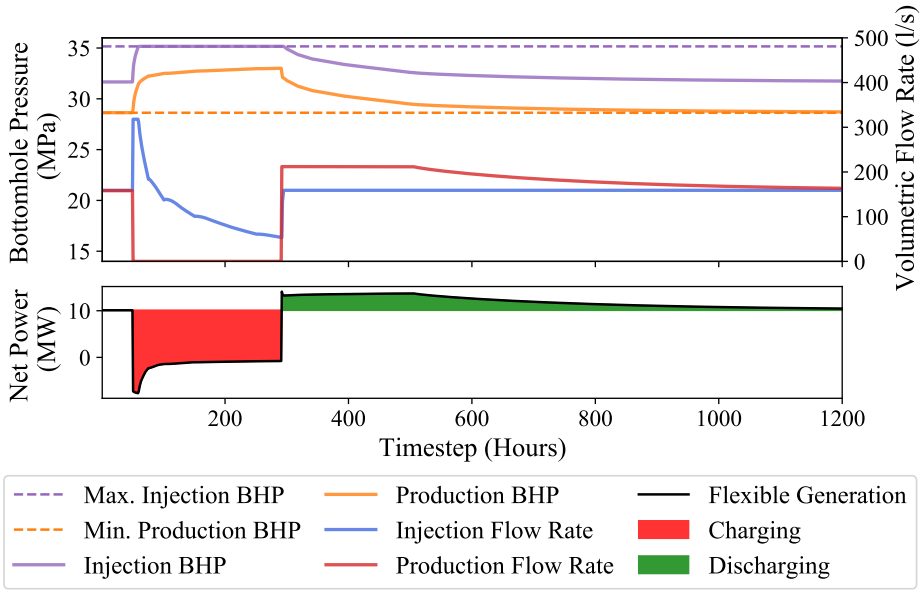

Figure 8: Operational decisions and net electrical output under a capacity-optimized charge-discharge cycle, for the base case model.

These results indicate that under baseline assumptions the subsurface reservoir of a fully flexible plant can store and discharge up to 159 MWh of electricity per MW of baseload surface capacity. Assuming that the "dis-

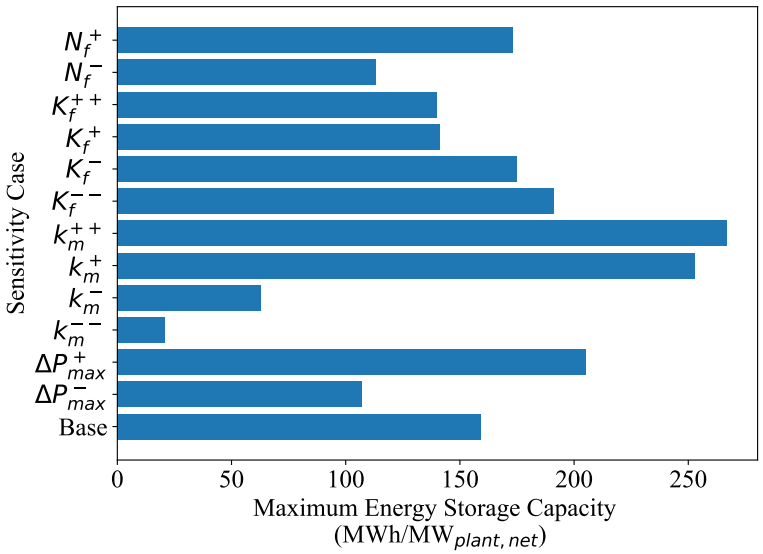

Figure 9: Maximum energy storage capacity per MW of baseload plant capacity for a flexible EGS plant under various sensitivity cases.

charge capacity" of IRES is roughly equivalent to the extra surface capacity built, this implies a storage duration in excess of 450 hours. This figure falls well within the range described by Sepulveda et al. [49] as ideal for long-duration energy storage technologies in decarbonized electricity systems.

Sensitivity analysis indicates that storage capacity has a positive relationship with the maximum allowable reservoir pressure. Matrix permeability has a strong effect on storage capacity, with very low matrix permeability showing significantly reduced storage durations. This finding is in line with results presented in Section 3.3. Fracture conductivity has a counter-intuitive effect on storage capacity, as lower values for this parameter lead to larger capacities. In these low fracture conductivity cases, changes in flow rate at one well have a significantly muted effect on BHP at the other wells. This effect leads to a delinking of injection and production BHPs, allowing the system to raise production BHP by a greater amount without violating the injection well BHP cap. Finally, results indicate that storage capacity scales with the number of fractures. While adding fractures increases total reservoir transmissivity and thereby reduces the delinking effect noted above, the increased storage potential due to a larger contact area with the rock matrix

outweighs this effect.

These results are idealized in the sense that real electricity prices do not necessarily incentivize capacity-optimized charge-discharge cycles hundreds of hours long. It should also be noted that, when analyzing storage capacity, it is difficult to quantify the state of charge for this system in a consistent manner. Reservoir pressure is limited by the injection BHP cap, but a combination of production BHP and flow rate histories determines the total discharge potential at any given time. Nevertheless, the results presented in Fig. 9 represent good ballpark estimates of the maximum energy storage capacity provided by an EGS reservoir under different subsurface conditions.

3.5. Discussion of In-Reservoir Energy Storage

As an energy storage technology, fully flexible geothermal power is fairly unique. It has significant charging power capacity, equivalent to the capacity of the base geothermal plant plus any additional load from increased injection pumping. This parasitic load can be increased significantly during times of very low or negative electricity prices, allowing for rapid pressurization of the reservoir at the cost of round-trip storage efficiency. Charging rate is limited only by the capabilities of the injection pumps and pressure ratings of surface piping and wellheads, all of which are fairly low-cost relative to other plant components [50, 51]. The storage discharge power capacity is more constrained, being limited by the size of the surface plant and grid interconnection as well as by the current level of reservoir pressurization. Binary-cycle geothermal plants have a relatively high specific cost (on the order of $2,000/kW) [50, 51], which limits the economically viable discharge capacity of a flexible geothermal plant. As discussed in Section 3.1, optimal surface capacities for flexible plants are generally not significantly larger than those for baseload plants. This economic constraint means that flexible geothermal is ill suited to delivering large injections of power over short timescales. However, effective "discharge" capacity can also be increased (at generally lower cost, depending on location) by oversizing transmission interconnection capacity and cutting injection pumps to boost net generation during high price periods, even without increasing gross generation capacity. As illustrated above, economically optimized round-trip efficiencies for flexible EGS plants are in the same range as those for today's leading grid-scale storage technologies. Table 5 compares the fundamental parameters of geothermal IRES to those of a number of competing grid-scale storage technologies.

What makes EGS energy storage unique is its large energy capacity, which comes essentially free of charge as an inherent property of an engineered geothermal reservoir. Low-cost energy capacity is the most important characteristic of effective long-duration energy storage technologies [49], and enables the hundred-hour-plus charging and discharging behaviors observed in Fig. 3. The energy storage provided by these plants is therefore extremely competitive, providing an option that is in many ways superior to other grid-scale storage technologies. Its primary downside is that it can also only be accessed via construction of a full-scale geothermal power plant. Its economic viability is therefore tied to that of next-generation geothermal power. However, if geothermal systems exploiting advanced drilling and stimulation techniques can be successfully developed in near-field locations and harness cost reductions from both oil and gas sector spillovers, progressive learning-by-doing in well completion and stimulation [37], and economies of scale in binary ORC turbine production [52], geothermal costs may become steadily lower over time. In this case, the ability to take advantage of such effective energy storage can significantly improve the economics of future geothermal projects, as is demonstrated in this paper, with increased revenue from flexible operation potentially expanding the range of economically-viable early-stage projects.

Table 5: Comparison of EGS IRES cost and efficiency parameters with future projections for leading grid-scale storage technologies. Competing technology parameters are taken from Sepulveda et al. [49], and are subject to geological and geographic constraints. Lithium-ion battery costs are projections for the year 2040 taken from the NREL ATB 2020 [53].

Technology	Power Capacity Cost ($/kW)	Energy Capacity Cost ($/kWh)	Round-Trip Efficiency (%)
EGS IRES	1100-2600	< 1	61-91
Pumped Hydro	600-2000	20+	70-85
Compressed Air	600-1150	1-30+	42-67
Power-H_2-Power (Fuel Cell)	440-3400	1-15+	20-46
Firebrick Resistance-Heated Energy Storage	930-1150	5-10	49-54
Vanadium Redox Flow Battery	270-600	40-200	65-80
Lithium-Ion Battery	82-180	94-206	85

4. Conclusions and Future Work

While geothermal power has significant potential to contribute to a zero-carbon electricity grid, the technology's historically inflexible generation profile limits its usefulness and economic appeal in systems with high VRE penetration. In this paper, we demonstrate that by exploiting the hydraulic and geomechanical properties of a confined geothermal reservoir, an EGS power plant can provide flexible generation and energy storage services that significantly enhance its economic value. We develop a novel modeling framework which accurately represents pressure and flow behaviors within an EGS reservoir and optimizes operations and investments to maximize the revenue of a geothermal power plant. The results presented here indicate that under the right conditions, an EGS reservoir can efficiently store hundreds of megawatt-hours of energy per MW of surface capacity without significantly increasing reservoir pressure. This large energy storage capacity is an inherent property of a confined reservoir, and therefore comes at no extra cost relative to a baseload geothermal plant. By taking advantage of this capability to provide flexible generation and energy storage, EGS plants can improve their energy value by a large amount relative to baseload geothermal plants. If this additional value can be translated into plant revenues via well-constructed energy and capacity markets or power-purchase agreements, flexible operations and energy storage can effectively raise the price point at which EGS power can compete as an energy source. This extra financial breathing room could be crucial to the economic success of early EGS projects, which represent an important step on the experience curve that could unlock development of much more significant "deep EGS" resources.

We find that flexibility and energy storage are more valuable in electricity markets with high VRE penetration, where large fluctuations in electricity prices provide opportunities for arbitrage. Sensitivity analysis shows that while baseload plant energy production varies somewhat, the degree of value added by full flexibility is fairly insensitive to variation in most subsurface parameters and surface plant costs. The greatest impact is observed in the very low matrix permeability case, which significantly reduces both the total energy storage capacity of the reservoir and the revenue improvements that can be achieved through flexible operation. These results indicate that flexible operations and energy storage can improve the value of EGS projects across a wide range of subsurface conditions, but that these conditions will need to be well-characterized in order to accurately assess a site's flexible

potential.

Our results are based on numerical reservoir simulations of a triplet well configuration with a reservoir management strategy involving a ratio of two production wells per injection well, and a uniform series of vertical fractures. It is likely that different reservoir designs will see different energy storage capacities and efficiencies. For example, reservoirs with larger stimulated volume per unit of flow rate will likely see larger storage capacities but slower charging times. However, as long as the engineered reservoir remains confined, the results presented here should remain qualitatively accurate. Extending this reasoning, it may be possible to exploit IRES in geothermal systems that would not traditionally be classified as "EGS." In formations with much higher natural permeability and no artificial fractures, a large number of triplets could be organized so as to impose artificial flow barriers on the more central wells, creating an effectively confined system like that proposed in Buscheck et al. [31]. Given the observed positive effect of reduced matrix permeability on storage potential, high-permeability systems may derive even greater benefits from flexible operation than traditional EGS. The potential to engineer and optimize operations of flexible geothermal systems across a wider range of possible subsurface conditions should be explored in future work.

A subject not investigated in this paper is the potential for flexible operating strategies to produce stresses that negatively affect well and reservoir integrity over the lifetime of a geothermal plant. It is possible, as discussed above, that pressurization of the reservoir and frequent changes in flow rates could increase the risk of induced seismicity. Well damage due to thermal cycling has also been cited as a potential downside of steam flow curtailment at The Geysers [54], though this problem may be less severe for liquid-dominated systems like those investigated here. Finally, modulation of injection and production rates may produce unforeseen issues with mineral precipitation and scaling, increasing the costs associated with flexible operations and IRES.

Despite the high level of detail captured by the reservoir simulation software used in this study, only at-scale field testing can fully confirm the viability of IRES as an EGS operating strategy. Though the basic principles of IRES were demonstrated successfully at Fenton hill, the risks of operating a new EGS field in a fully flexible mode without prior field testing are extremely high. This work represents an initial screening effort designed to estimate the incremental value of IRES under reasonable assumptions, and the significant

potential benefits demonstrated here suggest that further research and field demonstration are warranted. Extensive field validation of flexible operating strategies to assess the long-term impacts of flexible operations on reservoir performance and surface plant O&M costs, as well as the associated seismic risk, should be explored as a next step. Results from field testing can be used to further refine the modeling tools developed here, leading to more accurate assessments of value. It is likely that multiple demonstrations in different lithologies will be required before this technology can be reliably deployed at scale.

The work presented in this paper is designed to assess the value of flexible operations and energy storage for early EGS projects, and does not focus on electricity systems under deep decarbonization. Moving toward entirely carbon-free electricity would almost certainly drive greater deployment of variable wind and solar resources [12, 13, 14], which would lead to even greater benefits from geothermal storage and flexibility. However, it is likely that any successfully deployed early EGS projects will have entered the market well before this level of decarbonization is achieved. Because the fixed price series analysis used in this work assumes very low levels of flexible EGS market penetration, it is of limited use in quantifying the long-term value and deployment potential of flexible geothermal power under such scenarios. An accurate analysis of this long-term potential must capture the ability of flexible geothermal plants deployed at scale to influence the price of electricity through their operational decisions, as well as the diminishing marginal returns associated with increasing deployment of a specific energy technology, which apply especially strongly to energy storage technologies [36]. To this end, the optimization model developed for this paper is designed in such a way that it can be incorporated, with some reductions in complexity, into a larger long-term electricity system capacity expansion model. The use of capacity expansion modeling to analyze the long-term value and deployment potential of flexible geothermal power with energy storage will be the primary focus of our research on this subject going forward.

Acknowledgements

This work was supported by the US Department of Energy Office of Science SBIR program under Award No. DE-SC0020823, and by Princeton University's Carbon Mitigation Initiative. The authors thank Prof. Michael Celia for useful discussions.

Appendix A. Computational modeling and flexible geothermal reservoir simulation

In this work, we use a computational geothermal reservoir simulator to evaluate the technical feasibility of the in-reservoir energy storage operational strategy. We use a commercial reservoir simulation software package called ResFrac, which is capable of solving the coupled physical processes involved in geothermal reservoir production, including fluid flow in porous and fractured media, fluid flow in complex wellbores, heat transfer, and mechanical deformation of the subsurface [41, 42]. Here, we provide a brief overview of the governing equations and numerical methods used in the reservoir simulator. A more detailed description of the simulator is provided in the ResFrac users manual [42].

The simulator used in this study is a fully-compositional, thermal, and geomechanical reservoir model. The simulator integrates fluid flow in the wellbores, fluid flow in the reservoir, heat transfer in the reservoir, and mechanical deformation of the pore volume and fractures in the subsurface. The governing equations involve momentum balance for flow in the wellbore, mass balance for flow in the reservoir, energy balance for heat transfer in the reservoir, and momentum balance for mechanical deformation of the reservoir.

The system is discretized numerically using one-dimensional elements along the wellbore, three-dimensional volumetric elements for the reservoir matrix, and two-dimensional surface area elements for the fractures. Fluid flow and heat transfer are calculated using a finite volume method. Fracture deformation is calculated using a boundary element method. In this study, we use a Cartesian mesh for the reservoir matrix volume and a fracture mesh of rectangular elements. Solving this system of equations allows us to calculate fluid pressure along the wellbore (along with flowing friction), the fluid pressure distribution in the reservoir and fracture volume, the temperature distribution in the reservoir and fracture volume, and the mechanical deformation of the fractures.

In our simulations, the reservoir is assumed to be fully saturated with single-phase water. Thermoelastic and poroelastic stresses caused by temperature and pressure changes in the matrix are neglected in this study, therefore fracture deformation is caused by changes in fluid pressure within the fracture as well as mechanical interaction between fractures.

Appendix B. Development and Validation of the Linear Optimization Model

While simulation results are useful for evaluating the performance of a flexible geothermal reservoir under an exogenously determined operational strategy, the simulation software is too computationally intensive to allow for endogenous optimization of plant operations. Such an optimization would ideally be performed within a linear programming (LP) framework, which enables quick solutions to complex optimization problems with tens of thousands of decision variables and constraints. An LP formulation is also desirable because it allows the plant-level flexible geothermal model developed in this paper to be easily incorporated into a larger electricity system capacity expansion model (typically formulated as an LP or a mixed-integer LP), which is a priority for future work.

The LP formulation used to optimize investments and operations for a flexible geothermal power plant must accurately represent the pressure and flow behaviors observed in numerical simulations, ideally being capable of reproducing simulation results when executing an identical operational strategy. It must do so while remaining computationally lean and entirely linear, neglecting most of the complicated physics included in the numerical simulations. The following subsections describe how a formulation that meets these requirements was developed and validated.

Appendix B.1. Reservoir Pressure Behavior

Our approach to capturing pressure behavior in response to pumping takes advantage of several principles from the field of groundwater hydrology. The first, and most important, is that the transient pressure response at any fixed point in a static subsurface reservoir to constant pumping on a well penetrating that reservoir is a consistent function directly proportional to the pumping rate [55]. That is to say, pumping at double the rate on a well will result in double the transient pressure response in the reservoir. Thus, if we know the transient pressure response curve corresponding to pumping on one of the wells in a flexible geothermal reservoir at a single constant rate, we can find the pressure response to pumping on that well at any constant rate.

To extract this information, we run specially-designed numerical simulations for every set of subsurface conditions examined in this paper. In

each simulation, the geothermal reservoir is allowed to operate under steady-state conditions (i.e. at a constant injection rate with no production curtailment) for a period of five years in order to ensure that no transient behaviors are present. The production rate is then instantaneously lowered by a pre-prescribed amount, and kept at that level for a period of 240 hours. The system is allowed to come back into equilibrium, and the injection rate is then increased by the same amount for an identical period of time. The transient pressure responses at the injection and production well bottomholes are recorded during both of these periods. We create piecewise linearizations for each of these four pressure response functions, at hourly timesteps, and normalize each function to a unit pumping rate.

These functions give the pressure responses to constant pumping rates, but to have a useful model of a flexible geothermal system we must accurately capture the response to variable pumping rates. The technique we use to accomplish this is linear superposition of pressure transients. This technique's basic principle states that the transient pressure response to multiple stepwise changes in pumping rate on a given well is simply the superposition of the individual pressure responses to each of the stepwise changes taken in isolation. The superposition technique is outlined in Reilly et al. [56], and is valid for groundwater problems where the governing equations for flow and boundary conditions are universally linear. These conditions are generally satisfied by confined reservoirs like those investigated in this paper. One possible nonlinearity comes from the dilation of fracture apertures in response to increased reservoir pressure, which leads to non-constant fracture conductivity. As will be demonstrated, this nonlinearity is small and does not meaningfully affect the accuracy of the superposition approach.

Based on the principle of superposition, we create a set of constraints to model the injection and production well bottomhole pressures (BHPs) as functions of the injection and production rates at previous timesteps. These are constraints C.4a and C.4b in Section Appendix C. They express BHP for each well as the linear superposition of the transient pressure responses to changes in injection and production rates over n previous timesteps. For this work, we choose $n = 200$, as the second derivative of the pressure response function is negligible after 200 hours. Limiting the number of timesteps referenced in this constraint reduces the runtime of the overall LP. Beyond this point, we assume that the pressure changes at a constant rate, denoted ω^{ss} in the model formulation. The same value of ω^{ss} is used for both wells, as both experience convergent long-term behavior.

Appendix B.2. Maximum Production Flow Rate

Reservoir simulation outputs are also used to calibrate the relationship between production BHP and the maximum achievable production flow rate at a given time step. Physically, production flow rate as a function of production BHP is given by Bernoulli's equation for turbulent pipe flow with friction:

$$\frac{(P_{BH} - P_{WH})}{\rho g} + \Delta z = \frac{v^2}{2g} + H_{friction}, \tag{B.1}$$

Where P_{BH} is the production bottomhole pressure, P_{WH} is the minimum allowable value of production wellhead pressure, v is flow velocity in the well, z is the vertical length of the well, and $H_{friction}$ is the major head loss due to friction, given by the Darcy-Weisbach Equation:

$$\frac{H_{friction}}{L} = \frac{f_D v^2}{2gD}, \tag{B.2}$$

Where L is the length of the well, f_D is the Darcy friction factor, and D is the diameter of the well. The maximum achievable production flow rate $Q_{prodmax}$ for a given value of P_BH is directly proportional to v as given by the above equations. Rather than explicitly calculating the friction factor and other quantities to find the dependence of $Q_{prodmax}$ on P_{BH}, we use these equations to derive a fit of the form:

$$Q_{prodmax} = \sqrt{a \times P_{BH} + b}, \tag{B.3}$$

where a and b are unknown fit constants. We fit reservoir simulation results to this function to find values for a and b, thereby expressing production flow rate as a function of production BHP. Equation B.3 is nonlinear, so we cannot explicitly include it as a constraint in our LP model. Instead, because the curve is highly linear in the region with which we are concerned, we approximate it via a single linear constraint.

Appendix B.3. Validation of the Pressure and Flow Formulations

As stated above, the goal in developing a LP optimization model for flexible geothermal was to be able to reproduce simulation results with a high degree of accuracy. To validate the LP pressure and flow formulations described in Sections Appendix B.1 and Appendix B.2, we force our optimization model to perform the same set of operations as in the original

numerical simulations. Model outputs plotted alongside simulation outputs are shown in Fig. 2 of the main paper, and in Fig. B.10. There is strong agreement between the model and simulation results during both long and repeated short charging cycles. The fact that agreement is strong even during periods of variable production rate serves as a validation of the superposition approach described in Section Appendix B.1 and the linearization in Section Appendix B.2, and confirmation that any nonlinearities present in the system are not very significant.

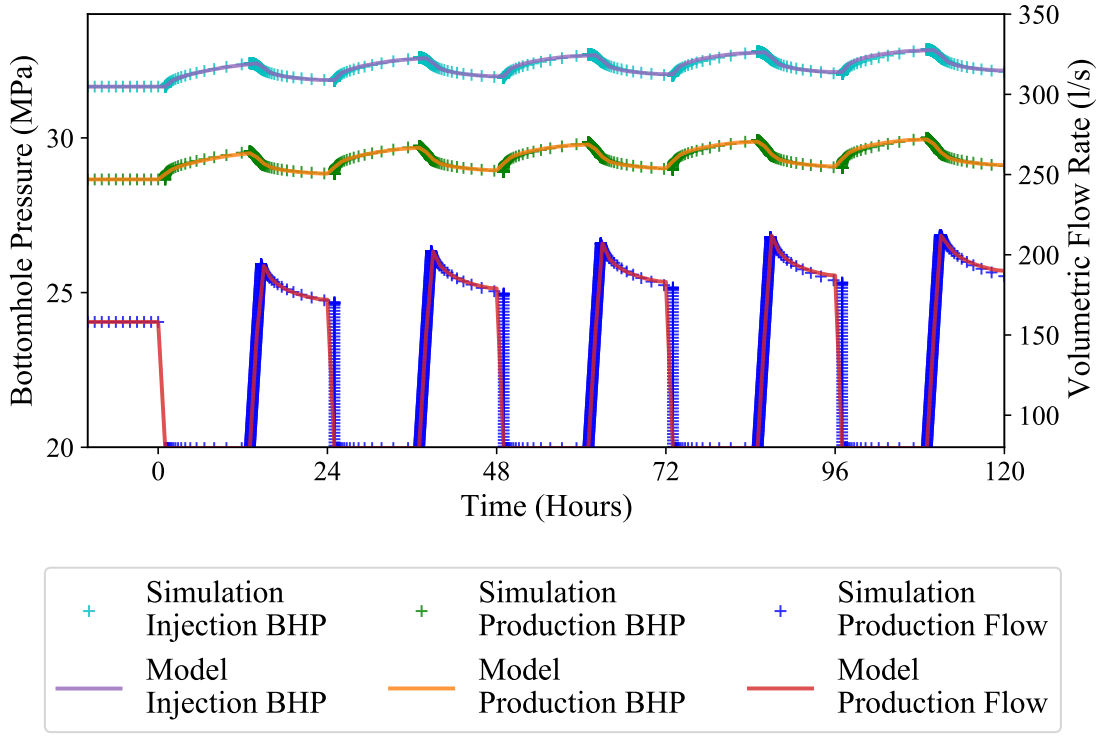

Figure B.10: The LP optimization model and the numerical simulation executing a series of daily production cycles. Simulation results are shown as point data, while model results are shown as continuous data.

Appendix B.4. Injection Pumping Requirements

The optimization model must endogenously calculate the parasitic load due to injection pumping, and by extension the injection WHP required to pump at a given injection rate. This effect is considered separately from the

injection well BHP, which is calculated via the linear superposition approach described in the previous section. The injection WHP at a given timestep is calculated as the sum of the injection BHP and the pressure differential ΔP_i across the injection well, the latter of which depends exclusively on the injection rate. The pressure differential is a nonlinear function of the injection rate, governed by the Bernoulli equation as described in Section Appendix B.2, and is found explicitly by fitting this equation to reservoir simulation results. Because this function is highly nonlinear, a step function is developed to represent it in the LP model. The range of possible injection pumping rates is divided into 53 l/s intervals, and it is assumed that pumping at any point in each interval induces a ΔP_i equal to the value of the nonlinear function at the uppermost point of that interval. The practical result of this modeling choice is that the value of injection WHP, which increases nonlinearly with injection rate, is overestimated in the intervals between the calibration injection rates. This choice biases the model towards pumping at exactly those rates, where the distortion is minimal, but still allows for continuous modulation of injection rate when such a strategy is optimal. The distortion could be minimized by including more injection "segments," but including too many of these would increase the model size significantly. In our model, we choose to use six injection segments as a compromise between these competing interests. Injection rate is capped at double the steady-state injection rate, at which point injection wellhead pressure begins to become excessive.

Not only is the physical relationship between injection WHP and injection rate nonlinear, but the relationship between these quantities and pumping power is as well. Pumping power is directly proportional to the product of injection rate and injection WHP, a relationship which cannot be explicitly modeled in an LP formulation if both quantities are variable. To capture the parasitic load from injection we employ a linear approximation which overestimates the pumping power to a small degree. The explicit constraint formulation is detailed in Section Appendix C. Overall, our LP model is formulated in such a way that it always returns a value for injection pumping power greater than or equal to the true value for the same injection rate and injection WHP. Because injection pumping power is a small portion of the plant's net power output ($\sim$10%), this overestimation has only a minor effect on model results. The effect of this choice is that the linear optimal objective (and therefore the calculated benefits attributable to flexibility), will be a fairly tight lower bound for the true nonlinear optimum.

Appendix B.5. Power Plant Operational Constraints

Several abstractions are introduced in order to accurately represent the Organic Rankine Cycle surface plant within a linear optimization framework. First, the plant is assumed to be capable of operating continuously from 0-110% capacity at a constant efficiency. ORCs, unlike large thermal generators, have very quick startup times. Thus, they are capable of rapidly and efficiently adjusting their output continuously over the range of 10-100% capacity and in a stepwise manner from 0-10%. Removing this lower discontinuity has a minimal effect on model outputs (the model very infrequently chooses to produce in this region, typically going all the way to zero), while allowing us to keep the model linear and continuous. The extra 10% peaking capacity is justified by the fact that ORCs can operate at high efficiencies off-design, and have been shown to be capable of accepting up to 10% higher geofluid mass-flow rates with minimal efficiency loss [43].

Plant power output is determined based on the geofluid mass flow rate, difference in enthalpy between production and injection conditions, and net plant thermo-electric conversion efficiency (including plant parasitic loads, but neglecting wellfield pumping power). Plant efficiency is calculated for given inlet and outlet temperatures based on results from genGEO, an open-source geothermal combined reservoir, well, power plant, cost, and financing simulator [57], presented in Adams et al. [50]. For the conditions used in this paper, namely an inlet temperature of 210 C and an outlet temperature of 70 C, net plant efficiency is 13.80%.

Appendix B.6. Cost and Financing Assumptions

Plant specific cost for the base case is calculated for the same set of conditions based on genGEO results, at \$1950/kW net. This cost does not include production pumps, which are not used in the design considered in this paper, and cost of the field gathering system. We assume a field gathering system cost of \$100/kW. Because only some plant component costs scale with production flow rate, and costs of others scale in nonlinear fashion, we assume that plant capacity oversizing has a specific cost equal to 80% that of the base plant. Injection pump specific cost is set based on genGEO parameters at \$400/kW, where this cost is in relation to the power consumed by the pump. For surface facilities financing, we assume that interest equal to 6% of plant overnight cost is accumulated during a one year construction period, and that during its 30 year capital recovery period the plant has a nominal weighted average cost of capital (WACC) of 5.5%, and a real

WACC of 2.93%. These assumptions result in an annual capital recovery factor of 5.1%. In addition to this annuitized investment cost, it is assumed that surface facilities oversizing leads to proportionately increased maintenance costs. These are calculated to be 1.8% of plant CAPEX annually, a value taken from the GETEM geothermal development simulator produced by NREL [51]. It should be noted that these maintenance costs assume the presence of a downhole production pump, which is not used in our model. The annual cost of taxes and insurance is set at 0.75% of plant CAPEX, a value also taken from GETEM. It is assumed that surface facilities oversizing does not result in increased labor costs. We further account for the cost of additional grid interconnection capacity. The capital cost of geothermal interconnection is set at $130/kW, with a capital recovery period of 60 years and a nominal WACC of 6.9%, as reported in Gorman et al. [58]. All financial information used in this paper is presented in 2019 $USD.

Appendix C. Optimization Model Formulation

The following sections present the explicit formulation of the LP optimization model used in this work. All parameter values are for the base-case model, and some vary between sensitivity cases.

Appendix C.1. Model Indices, Variables, Expressions, and Parameters

Table C.8: Model Parameters

Notation	Description
p^{cap1}	Baseload plant net electric generating capacity excluding injection pumping load, 11.1 MW
	Continued on next page

Table C.6: Model Indices

Notation	Description
$t \in [0, ..., 8760]$	Where t denotes an hour in the modeled weather year. Hour 0 sets initial conditions.
$n \in [1, ..., 6]$	Where n denotes one of six injection pumping levels.

Table C.8 – continued from previous page

Notation	Description
p^{cap2}	Baseload plant net electric generating capacity including injection pumping load, 10.1 MW
p^{cap3}	Baseload plant injection pumping power, 1.0 MW
p^{peak}	Peaking factor representing maximum usable geofluid flow, 1.1.
$p^{iBHPmin}$	Minimum and starting injection bottomhole pressure, 31.66 MPa.
$p^{iBHPmax}$	Maximum injection bottomhole pressure, 35.16 MPa.
$p^{pBHPmin}$	Minimum and starting production bottomhole pressure, 28.63 MPa.
$p^{i\Delta P}$	Pressure differential across injection well at steady-state injection rate, 26.17 MPa.
p^{iseg}	Range of each injection pumping interval, 53 l/s.
$p^{iWHPmin}$	Minimum injection wellhead pressure due to pumping in the 0-53 l/s interval, 2.34 MPa.
p^{iWHP2}	Additional injection wellhead pressure due to pumping in the 53-106 l/s interval, 1.18 MPa.
p^{iWHP3}	Additional injection wellhead pressure due to pumping in the 106-159 l/s interval, 3.14 MPa.
p^{iWHP4}	Additional injection wellhead pressure due to pumping in the 159-212 l/s interval, 5.90 MPa.
p^{iWHP5}	Additional injection wellhead pressure due to pumping in the 212-265 l/s interval, 9.44 MPa.
p^{iWHP6}	Additional injection wellhead pressure due to pumping in the 265-318 l/s interval, 13.76 MPa.
p^{iss}	Steady-state injection flow rate, 159.0 l/s.
p^{pss}	Steady-state production flow rate, 158.1 l/s.
$\alpha^{i}_{[0:200]}$	Hourly coefficients of the transient injection bottomhole pressure response function corresponding to changes in injection flow rate.
$\alpha^{p}_{[1:200]}$	Hourly coefficients of the transient injection bottomhole pressure response function corresponding to changes in production flow rate.
$\beta^{i}_{[1:200]}$	Hourly coefficients of the transient production bottomhole pressure response function corresponding to changes in injection flow rate.
$\beta^{p}_{[0:200]}$	Hourly coefficients of the transient production bottomhole pressure response function corresponding to changes in production flow rate.
ω^{ss}	Constant universal pressure response rate after 200 timesteps.
γ	Slope of the linear $Q_{prodmax}$ constraint.
δ	Intercept of the linear $Q_{prodmax}$ constraint.

Continued on next page

Table C.8 – continued from previous page

Notation	Description
η^{gf}	Surface plant specific power, 88.09 kW/(l/s)$_{geofluid}$.
η^{pump}	Injection pump power conversion factor, 1.14 kW/(MPa · l/s).
ρ_t	Electricity price at hour t.
c^{plant}	Annuitized fixed costs associated with surface plant oversizing, \$132804/MW$_{net,plant}$-yr.
c^{trans}	Annuitized fixed costs associated with interconnection oversizing, \$5629/MW-yr.
c^{pump}	Annuitized fixed costs associated with injection pump oversizing, \$32130/MW-yr.

Table C.7: Model Variables and Expressions

Notation	Description
y^{cap}	Surface plant net electric generating capacity.
y^{icap}	Surface plant grid interconnection capacity.
y^{pcap}	Injection pump power capacity.
x_t^{prod}	Volumetric production flow rate at hour t.
$x_{t,n}^{inj}$	Deviation from the steady-state injection rate at hour t and injection level n.
x_t^{iBHP}	Bottomhole pressure in the injection well at hour t.
x_t^{pBHP}	Bottomhole pressure in the production well at hour t.
e_t^{inj}	Volumetric injection flow rate at hour t.
e_t^{ipwr}	Parasitic load due to injection pumping at hour t.
e_t^{ppwr}	Net surface plant generation at hour t.

Appendix C.2. Objective Function

The Objective Function in Eq. (C.1) maximizes plant revenue over a weather year by co-optimizing investment and operational decisions.

$$\max_{x,y} \Bigg(\tag{C.1a}$$

$$\sum_{t\in[1:8760]} \Big((e_t^{ppwr} - e_t^{ipwr}) \cdot \rho_t \Big) - \tag{C.1b}$$

$$\Big((y^{cap} - p^{cap1}) \cdot c^{plant} + (y^{icap} - p^{cap2}) \cdot c^{trans} + (y^{pcap} - p^{cap3}) \cdot c^{pump} \Big) \Bigg) \tag{C.1c}$$

The method consists of maximizing the sum of all hourly operational revenues over the year (C.1b), while minimizing the annuitized costs of investments in surface plant, injection pump, and interconnection oversizing (C.1c). Operational revenue for any hour t is given by the product of the net electrical output of the plant, equal to the net power plant generation less the parasitic power used for injection pumping, and the price of electricity

at that hour. Total cost of surface plant oversizing is calculated as the difference between the oversized gross plant capacity and the baseload gross plant capacity, multipled by the annuitized specific cost of surface plant oversizing. Total cost of injection pump oversizing is the difference between the oversized injection pump maximum power and the baseload injection pump maximum power, multiplied by the annuitized specific cost of the injection pump. Total cost of interconnection oversizing is the difference between the oversized interconnection capacity and the baseload interconnection capacity, multiplied by the annuitized specific cost of interconnection.

Appendix C.3. Constraints

The optimization function defined in Eq. (C.1) is subject to different sets of constraints that define the feasible solution space for the decision variables. Without these constraints, the model would converge to unbounded levels of power production and the objective value would be infinite.

Appendix C.3.1. Variable Bounds

These constraints establish hard bounds on the decision variables of the optimization problem. Some variables are only bounded on one end.

$$y^{cap} \geq p^{cap1} \tag{C.2a}$$
$$y^{icap} \geq p^{cap2} \tag{C.2b}$$
$$y^{pcap} \geq p^{cap3} \tag{C.2c}$$
$$x_t^{prod} \geq 0 \qquad \forall t \in [0:8760] \tag{C.2d}$$
$$p^{iseg} \geq x_{t,n}^{inj} \geq 0 \qquad \forall t \in [0:8760], n \in [1:6] \tag{C.2e}$$
$$p^{iBHPmax} \geq x_t^{iBHP} \geq p^{iBHPmin} \qquad \forall t \in [0:8760] \tag{C.2f}$$
$$x_t^{pBHP} \geq p^{pBHPmin} \qquad \forall t \in [0:8760] \tag{C.2g}$$

Eq. (C.2a), Eq. (C.2b) and Eq. (C.2c) constrain the grid capacity of the surface plant built by the model to be larger than that of an inflexible baseload plant operating on the same wellfield, and the injection pump power capacity to be larger than that of a baseload plant. Eq. (C.2d) forces production rate to always be positive, preventing negative production during times of negative electricity prices. Eq. (C.2e) establishes bounds on each of the six injection pumping levels: each variable controls pumping across a

53 l/s range. Finally, Eq. (C.2f) and Eq. (C.2g) establish a maximum injection BHP and minimum production and injection BHPs. The maximum injection BHP represents a cap on reservoir pressurization due to concerns over induced seismicity, while the minimum BHPs (equal to the BHPs under steady-state inflexible operation) limit the pressure drawdown to prevent fracture closure.

Appendix C.3.2. Initial Conditions

Most of the state variables in the model are formulated in a manner that references previous states. The initial conditions set for all operational variables at timestep 0 represent the status of a plant in steady-state (i.e. inflexible) operation.

$$x_0^{prod} = p^{pss} \tag{C.3a}$$

$$x_{0,n}^{inj} = 0 \qquad \forall n \in [1:6] \tag{C.3b}$$

$$x_0^{pBHP} = p^{pBHPmin} \tag{C.3c}$$

$$x_0^{iBHP} = p^{iBHPmin} \tag{C.3d}$$

Eq. (C.3a) and Eq. (C.3b) set starting production and injection flow rates to their steady-state values, while Eq. (C.3c) and Eq. (C.3d) do the same for the production and injection bottomhole pressures.

Appendix C.3.3. Pressure Formulation

The constraints describing pressure evolution in response to changes in pumping are central to the accurate representation of geothermal flexibility. These represent the pressure at each well bottomhole as a superposition of linearized pressure response functions referencing changes in pumping rates during the previous 200 timesteps. The motivation and justification for this approach is described in greater detail in Section Appendix B.1.

$$\begin{aligned} x_t^{iBHP} =& x_{t-1}^{iBHP} + (e_t^{inj} - e_{t-1}^{inj}) \cdot (\alpha_0^i - \omega^{ss}) + \\ & \sum_{a \in [1:200]} \Big((e_{t-a}^{inj} - e_{t-a-1}^{inj}) \cdot (\alpha_a^i - \omega^{ss}) - \\ & (x_{t-a}^{prod} - x_{t-a-1}^{prod}) \cdot (\alpha_a^p - \omega^{ss}) \Big) + \\ & (e_{t-1}^{inj} - x_{t-1}^{prod}) \cdot \omega^{ss} \end{aligned} \qquad \forall t \in [1:8760] \tag{C.4a}$$

$$
\begin{aligned}
x_t^{pBHP} = x_{t-1}^{pBHP} - (x_t^{prod} - x_{t-1}^{prod}) \cdot (\beta_0^p - \omega^{ss}) + \\
\sum_{b \in [1:200]} \Big((e_{t-a}^{inj} - e_{t-a-1}^{inj}) \cdot (\beta_a^i - \omega^{ss}) - \\
(x_{t-a}^{prod} - x_{t-a-1}^{prod}) \cdot (\beta_a^p - \omega^{ss}) \Big) + \\
(e_{t-1}^{inj} - x_{t-1}^{prod}) \cdot \omega^{ss}
\end{aligned}
\qquad \forall t \in [1:8760] \qquad \text{(C.4b)}
$$

Eq. C.4a describes the injection BHP at hour t as a function of the injection BHP at the previous hour and the cumulative effects of injection and production flow rate changes at previous timesteps, and Eq. C.4b does the same for production BHP. The first line of each constraint references the pressure at the previous timestep, as well as an "instantaneous" (i.e. on a timescale much less than an hour) change in pressure due to pumping on the same well at the current timestep. The second and third lines capture the superimposed effects of all production and injection rate changes at the previous 200 timesteps. The last line references the difference between the net pumping rate into the reservoir at the previous timestep and the steady-state net pumping rate, which captures the lingering cumulative effects of changes in pumping at all previous timesteps. The development and validation of these pressure constraints are described in greater detail in Section Appendix B.1.

Appendix C.3.4. Production Rate and Generation

Production flow rate is limited by production well BHP, while *usable* production flow is constrained by the surface plant capacity and grid interconnection. The physical constraints on maximum production flow rate and the conversion between production flow and electrical power are described in greater detail in Section Appendix B.2.

$$
\begin{aligned}
e_t^{ppwr} &= x_t^{prod} \cdot \eta^{gf} && \forall t \in [1:8760] && \text{(C.5a)} \\
e_t^{ppwr} &\leq p^{peak} \cdot y^{cap} && \forall t \in [1:8760] && \text{(C.5b)} \\
e_t^{ppwr} - e_t^{ipwr} &\leq y^{icap} && \forall t \in [1:8760] && \text{(C.5c)} \\
x_t^{prod} &\leq \gamma \cdot x_t^{pBHP} + \delta && \forall t \in [1:8760] && \text{(C.5d)}
\end{aligned}
$$

Eq. (C.5a) sets the power generation associated with a given production flow rate to be the product of the flow rate and the surface plant specific

power. Eq. (C.5b) constrains this power to be less than the product of the net generating capacity of the surface plant and the peaking factor. Eq. (C.5c) constrains the plant's total net generation, equal to generation less parasitic load, to be less than the capacity of the its grid interconnection at all timesteps. Eq. (C.5d) bounds the production flow rate from above based on a linearized nonlinear constraint, as detailed in Section Appendix B.2.

Appendix C.3.5. Injection Rate and Parasitic Load

Injection pumping rate and the resulting parasitic load are the most difficult quantities to capture in a LP model, as the actual physical relationships are highly nonlinear. We formulate the injection load in such a way that it is always greater than or equal to the actual load that would exist at the same pumping rate and wellhead pressure.

$$e_t^{inj} = p^{iss} - \sum_{n\in[1:3]} x_{t,n}^{inj} + \sum_{n\in[4:6]} x_{t,n}^{inj} \qquad \forall t \in [1:8760]$$

(C.6a)

$$x_{t,3}^{inj} \geq x_{t,2}^{inj} \geq x_{t,1}^{inj} \qquad \forall t \in [1:8760]$$

(C.6b)

$$x_{t,4}^{inj} \geq x_{t,5}^{inj} \geq x_{t,6}^{inj} \qquad \forall t \in [1:8760]$$

(C.6c)

$$x_{t,[1:3]}^{inj} + x_{t,[4:6]}^{inj} \leq p^{iseg} \qquad \forall t \in [1:8760]$$

(C.6d)

$$\begin{aligned} e_t^{ipwr} = {} & (x_t^{iBHP} - p^{i\Delta P}) \cdot \eta^{pump} \cdot p^{iss} - \\ & p^{iWHPmin} \cdot \eta^{pump} \cdot x_{t,1}^{inj} - \\ & (p^{iWHPmin} + 2p^{iWHP2}) \cdot \eta^{pump} \cdot x_{t,2}^{inj} - \\ & (p^{iWHPmin} + 3p^{iWHP3} - 2p^{iWHP2}) \cdot \eta^{pump} \cdot x_{t,3}^{inj} + \\ & (p^{iBHPmax} - p^{i\Delta p} + 4p^{iWHP4} - 3p^{iWHP3}) \cdot \eta^{pump} \cdot x_{t,4}^{inj} + \\ & (p^{iBHPmax} - p^{i\Delta p} + 5p^{iWHP5} - 4p^{iWHP4}) \cdot \eta^{pump} \cdot x_{t,5}^{inj} + \\ & (p^{iBHPmax} - p^{i\Delta p} + 6p^{iWHP6} - 5p^{iWHP5}) \cdot \eta^{pump} \cdot x_{t,6}^{inj} \end{aligned} \qquad \forall t \in [1:8760]$$

(C.6e)

$$e_t^{ipwr} \leq y^{pcap} \qquad \forall t \in [1:8760]$$

(C.6f)

$$\sum_{t\in[1:8760]} e_t^{inj} \leq 8760 p^{iss}$$

(C.6g)

Eq. (C.6a) formulates injection rate at hour t in terms of deviations from the steady-state injection rate, p^{iss}. Three variables $x_{t,[1:3]}^{inj}$ control reductions in injection rate, with each able to reduce total injection by 1/3 of the steady-state injection rate. $x_{t,[4:6]}^{inj}$ have a similar function, but each increase total injection by 1/3 of the steady-state injection rate. Each of these six $x_{t,n}^{inj}$ corresponds to a specific injection rate segment, i.e. 0-53 l/s, 53-106 l/s, etc. Eq. (C.6b) and Eq. (C.6c) ensure that these segments are activated

in the correct order. Eq. (C.6d) prevents the model from simultaneously raising and lowering the injection rate, which might generate additional revenue during times of negative electricity pricing. Eq. (C.6e) calculates the total injection pumping load at hour t. The first line expresses load due to pumping at the steady-state injection rate on the current injection BHP as the product of these quantities and the pump power factor η^{pump}. The next three lines deal with reductions in this load due to reductions in injection rate, which are calculated based on the minimum injection BHP and the current injection rate. The final three lines deal with increases in injection load due to increased injection rate, which are calculated based on the maximum injection BHP and the current injection rate. The result of this formulation is that reductions in parasitic load due to reductions in injection rate are always modeled as less than or equal to their true physical values, while additional injection load due to increased injection rate is always modeled as greater than or equal to its true value. Though it necessarily overestimates the parasitic load at most pressures and injection rates, this formulation is still able to capture most of the costs and benefits of increasing or decreasing injection rate, respectively. When injection rate is kept at its steady-state value, Eq. (C.6e) returns the exact value of the parasitic load. Eq. (C.6f) requires that the model build enough pump capacity to meet injection power requirements at all points throughout the year. Finally, Eq. (C.6g) requires that the average injection rate over the modeled year be less than or equal to the steady-state injection rate. This requirement ensures that the flexible geothermal plant experiences a thermal drawdown rate no greater than that of an inflexible plant.

Appendix D. Supplementary Results

Appendix D.1. Price Series Analysis

Figure D.11 shows price duration curves for all 16 historical and modeled future price series used in this study. Table D.9 provides statistics for each price series, including the number of hours for which prices are ≤ 0/MWh, and average daily and weekly standard deviations. Figs. D.12, D.13, and D.14 plot various statistics against the relative energy value improvement from in-reservoir energy storage for each price series. As shown in Fig. D.12, there is a fairly strong correlation between the number of hours with zero or negative prices and the level of energy value improvement from IRES. The correlation between the standard deviations and the level of energy value

improvement is weaker, with the daily standard deviation being the stronger indicator.

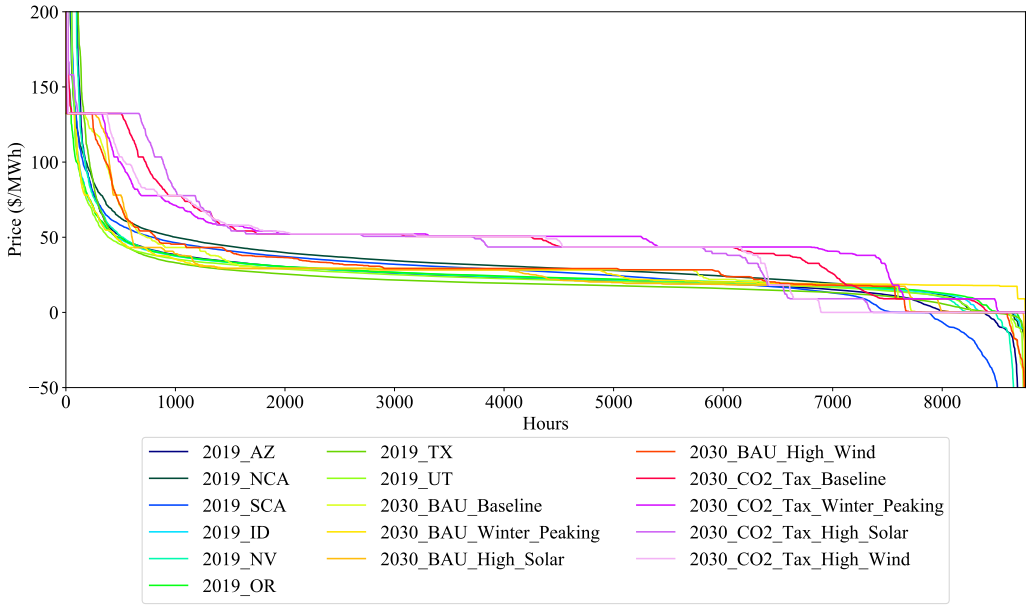

Figure D.11: Plotted price duration curves for 16 historical and modeled future price series.

Appendix D.2. Energy Storage Efficiency

Figure D.15 illustrates the yearly average round-trip efficiency for optimized operation on each price series under each sensitivity case. Values range from 61% to 91%, with an average across all runs of 81%.

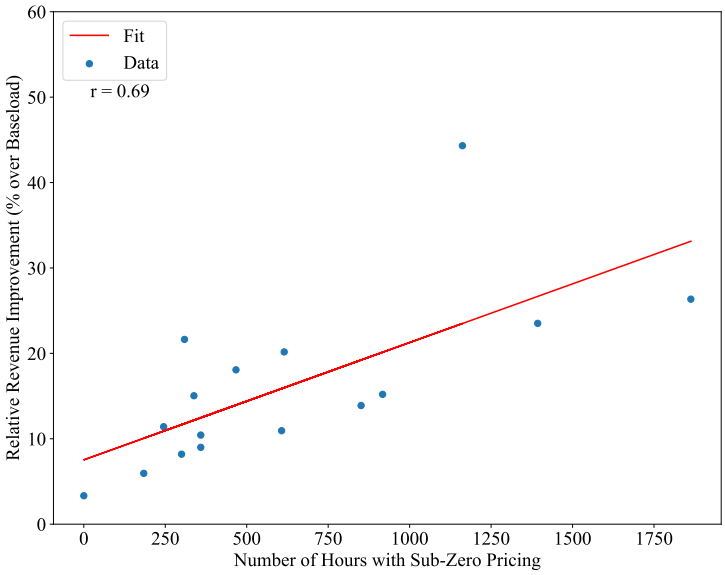

Figure D.12: Number of hours with electricity prices less than or equal to \$0/MWh, vs. relative geothermal energy value improvement from in-reservoir energy storage, for the base case model. A linear fit is shown in red, along with its r-value.

Table D.9: Statistics for historical and modeled future price series. All prices are given in $/MWh.

Price Series	Hours of ≤0 Pricing	Avg. Daily STD	Avg. Weekly STD
2019 AZ	615	46.3	73.2
2019 N-CA	359	23.4	37.7
2019 S-CA	1162	35.2	50.6
2019 ID	300	27.2	46.8
2019 NV	467	39.4	62.3
2019 OR	184	12.3	20.2
2019 TX	309	46.2	80.8
2019 UT	359	27.7	46.8
2030 BAU Baseline	851	22.0	23.4
2030 BAU Winter Peaking	0	15.9	21.9
2030 BAU High Solar	607	27.5	31.3
2030 BAU High Wind	917	23.6	30.3
2030 CO2 Tax Baseline	338	33.1	38.2
2030 CO2 Tax Winter Peaking	245	29.3	36.4
2030 CO2 Tax High Solar	1393	39.3	44.7
2030 CO2 Tax High Wind	1863	33.6	40.1

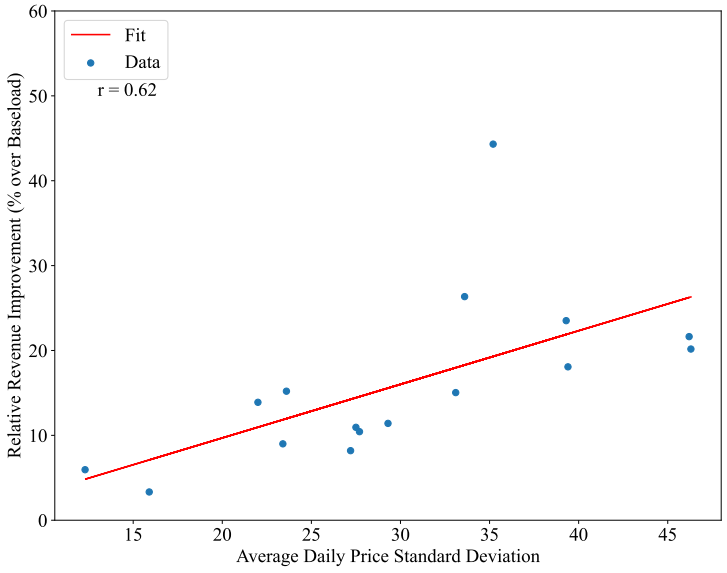

Figure D.13: Same as Fig D.12, showing correlation with daily average standard deviation of prices.

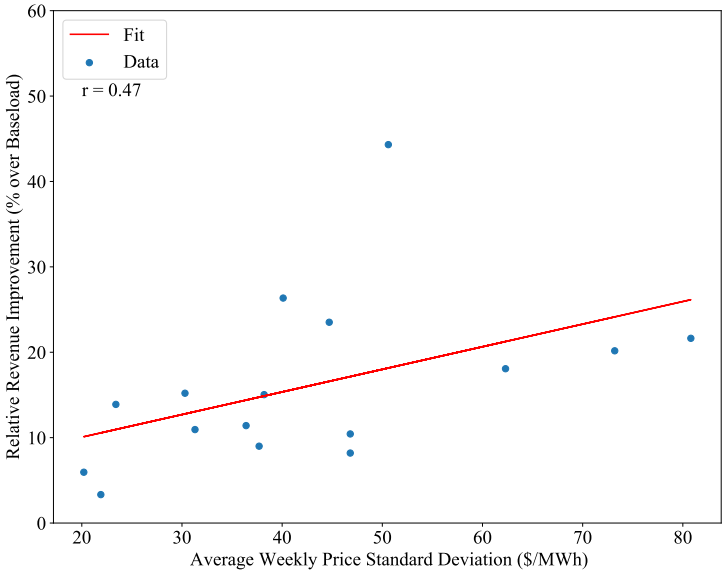

Figure D.14: Same as Fig D.12, showing correlation with weekly average standard deviation of prices.

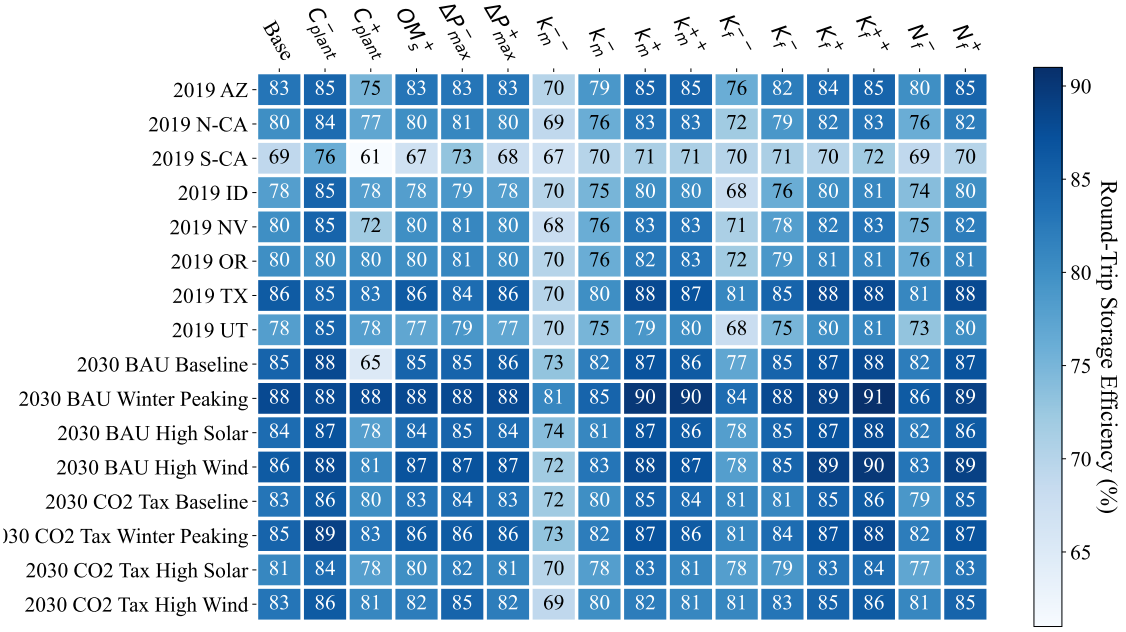

Figure D.15: Round-trip efficiency for in-reservoir energy storage across all price series and sensitivity cases.

References

[1] N. Sepulveda, J. Jenkins, F. de Sisternes, R. Lester, The role of firm low-carbon electricity resources in deep decarbonization of power generation, Joule 2 (2018) 2403–2420. doi:10.1016/j.joule.2018.08.006.

[2] E. Baik, K. P. Chawla, J. D. Jenkins, C. Kolster, N. S. Patankar, A. Olson, S. M. Benson, J. C. Long, What is different about different net-zero carbon electricity systems?, Energy and Climate Change 2 (2021) 100046. URL: https://www.sciencedirect.com/science/article/pii/S2666278721000234. doi:https://doi.org/10.1016/j.egycc.2021.100046.

[3] R. I. McDonald, J. Fargione, J. Kiesecker, W. M. Miller, J. Powell, Energy sprawl or energy efficiency: Climate policy impacts on natural habitat for the united states of america, PLOS ONE 4 (2009) 1–11. URL: https://doi.org/10.1371/journal.pone.0006802. doi:10.1371/journal.pone.0006802.

[4] Annual Energy Outlook 2021, Technical Report, U. S. Energy Information Agency (EIA), Washington, D.C., 2021.

[5] Initial Results from the 2020 U.S. Geothermal Power Production and District Heating Market Report, Technical Report, National Renewable Energy Laboratory (NREL), Golden, CO, 2021.

[6] C. Williams, M. Reed, R. Mariner, A Review of Methods Applied by the U.S. Geological Survey in the Assessment of Identified Geothermal Resources, Technical Report 2008-1296, U.S. Geological Survey (USGS), Menlo Park, CA, 2008.

[7] C. Williams, M. Reed, R. Mariner, J. DeAngelo, S. Galanis, Assessment of Moderate- and High-Temperature Geothermal Resources of the United States, Technical Report 2008-3082, U.S. Geological Survey (USGS), Menlo Park, CA, 2008.

[8] The Future of Geothermal Energy, Technical Report INL/EXT-06-11746, Idaho National Laboratory, Idaho Falls, ID, 2006.

[9] C. Augustine, Update to enhanced geothermal system resource potential estimate, 2016. Presented at the 40th GRC Annual Meeting, Sacramento, CA, 2016.

[10] GeoVision, Technical Report, U.S. Department of Energy (DOE), 2019.

[11] B. Matek, Flexible opportunities with geothermal technology: Barriers and opportunities, The Electricity Journal 28 (2015) 45–51.

[12] M. Jafari, M. Korpås, A. Botterud, Power system decarbonization: Impacts of energy storage duration and interannual renewables variability, Renewable Energy 156 (2020) 1171–1185. URL: https://www.sciencedirect.com/science/article/pii/S0960148120306820. doi:https://doi.org/10.1016/j.renene.2020.04.144.

[13] E. Larson, C. Greig, J. Jenkins, E. Mayfield, A. Pascale, C. Zhang, J. Drossman, R. Williams, S. Pacala, R. Socolow, E. Baik, R. Birdsey, R. Duke, R. Jones, B. Haley, E. Leslie, K. Paustian, A. Swan, Net-Zero America: Potential Pathways, Infrastructure, and Impacts, 2020.

[14] J. H. Williams, R. A. Jones, B. Haley, G. Kwok, J. Hargreaves, J. Farbes, M. S. Torn, Carbon-neutral pathways for the united states, AGU Advances 2 (2021) e2020AV000284. URL: https://agupubs.onlinelibrary.wiley.com/doi/abs/10.1029/2020AV000284. doi:https://doi.org/10.1029/2020AV000284. arXiv:https://agupubs.onlinelibrary.wiley.com/doi/pdf/10.1029/2020AV000284, e2020AV000284 2020AV000284.

[15] P. Denholm, M. O'Connell, G. Brinkman, J. Jorgenson, Overgeneration from Solar Energy In California: A Field Guide to the Duck Chart, Technical Report NREL/TP-6A20-65023, National Renewable Energy Laboratory (NREL), Golden, CO, 2015.

[16] A. D. Mills, T. Levin, R. Wiser, J. Seel, A. Botterud, Impacts of variable renewable energy on wholesale markets and generating assets in the United States: A review of expectations and evidence, Renewable and Sustainable Energy Reviews 120 (2020) 109670. URL: https://www.sciencedirect.com/science/article/pii/S1364032119308755. doi:10.1016/j.rser.2019.109670.

[17] P. D. Lund, J. Lindgren, J. Mikkola, J. Salpakari, Review of energy system flexibility measures to enable high levels of variable renewable electricity, Renewable and Sustainable Energy Reviews 45 (2015) 785–807. URL:

https://www.sciencedirect.com/science/article/pii/S1364032115000672. doi:https://doi.org/10.1016/j.rser.2015.01.057.

[18] P. Denholm, M. Hand, Grid flexibility and storage required to achieve very high penetration of variable renewable electricity, Energy Policy 39 (2011) 1817–1830. URL: https://www.sciencedirect.com/science/article/pii/S0301421511000292. doi:https://doi.org/10.1016/j.enpol.2011.01.019.

[19] H. Kondziella, T. Bruckner, Flexibility requirements of renewable energy based electricity systems – a review of research results and methodologies, Renewable and Sustainable Energy Reviews 53 (2016) 10–22. URL: https://www.sciencedirect.com/science/article/pii/S1364032115008643. doi:https://doi.org/10.1016/j.rser.2015.07.199.

[20] T. Mai, M. M. Hand, S. F. Baldwin, R. H. Wiser, G. L. Brinkman, P. Denholm, D. J. Arent, G. Porro, D. Sandor, D. J. Hostick, M. Milligan, E. A. DeMeo, M. Bazilian, Renewable electricity futures for the united states, IEEE Transactions on Sustainable Energy 5 (2014) 372–378. doi:10.1109/TSTE.2013.2290472.

[21] B. S. Palmintier, M. D. Webster, Impact of operational flexibility on electricity generation planning with renewable and carbon targets, IEEE Transactions on Sustainable Energy 7 (2016) 672–684. doi:10.1109/TSTE.2015.2498640.

[22] L. Jones, Renewable Energy Integration: Practical Management of Variability, Uncertainty, and Flexibility in Power Grids, 2 ed., Elsevier, 2017.

[23] A. Bloom, A. Townsend, D. Palchak, J. Novacheck, J. King, C. Barrows, E. Ibanez, M. O'Connell, G. Jordan, B. Roberts, C. Draxl, K. Gruchalla, Eastern Renewable Generation Integration Study, Technical Report NREL/TP-6A20-64472, National Renewable Energy Laboratory, Golden, CO, 2016.

[24] J. Jenkins, Z. Zhou, R. Ponciroli, R. Vilim, F. Ganda, F. de Sisternes, A. Botterud, The benefits of nuclear flexibility in power system operations with renewable energy, Applied Energy 222 (2018) 872–884. URL: https://www.sciencedirect.com/science/article/pii/S0306261918303180. doi:https://doi.org/10.1016/j.apenergy.2018.03.002.

[25] C. Linvill, J. Candelaria, C. Elder, The Value of Geothermal Energy Generation Attributes: Aspen Report to Ormat Technologies, Technical Report, Aspen Environmental Group, 2013.

[26] D. Millstein, P. Dobson, S. Jeong, The Potential to Improve the Value of U.S. Geothermal Electricity Generation Through Flexible Operations, Journal of Energy Resources Technology 143 (2020) 010905. URL: https://doi.org/10.1115/1.4048981. doi:10.1115/1.4048981. arXiv:https://asmedigitalcollection.asme.org/energyresources/article-pdf/143/1

[27] K. Goyal, Reservoir response to curtailment at the geysers, in: Proceedings of the 27th Workshop on Geothermal Reservoir Engineering, Stanford, CA, 2002.

[28] S. Green, J. McLennan, P. Panja, K. Kitz, R. Allis, J. Moore, Geothermal battery energy storage, Renewable Energy 164 (2021) 777–790. URL: https://www.sciencedirect.com/science/article/pii/S0960148120315081. doi:https://doi.org/10.1016/j.renene.2020.09.083.

[29] J. McTigue, G. Zhu, C. Turchi, Hybridizing a Geothermal Plant with Solar and Thermal Energy Storage to Enhance Power Generation, Technical Report NREL/TP-5500-70862, National Renewable Energy Laboratory, Golden, CO, 2018.

[30] M. Fleming, B. Adams, J. Randolph, J. Ogland-Hand, T. Kuehn, T. Buscheck, J. Bielicki, M. Saar, High efficiency and large-scale subsurface energy storage with co_2, in: Proceedings of the 43rd Workshop on Geothermal Reservoir Engineering, Stanford, CA, 2018.

[31] T. A. Buscheck, J. M. Bielicki, T. A. Edmunds, Y. Hao, Y. Sun, J. B. Randolph, M. O. Saar, Multifluid geo-energy systems: Using geologic CO2 storage for geothermal energy production and grid-scale energy storage in sedimentary basins, Geosphere 12 (2016) 678–696. URL: https://doi.org/10.1130/GES01207.1. doi:10.1130/GES01207.1. arXiv:https://pubs.geoscienceworld.org/gsa/geosphere/article-pdf/12/3/678/3334

[32] J. Ogland-Hand, J. Bielicki, B. Adams, T. Buscheck, M. Saar, Using sedimentary basin geothermal resources to provide long-duration energy

storage, in: Proceedings of the World Geothermal Congress 2020, Reykjavik, Iceland, 2021.

[33] D. W. Brown, D. V. Duchane, G. Heiken, V. T. Hriscu, Mining the Earth's Heat: Hot Dry Rock Geothermal Energy, Springer, 2012.

[34] F. J. de Sisternes, J. D. Jenkins, A. Botterud, The value of energy storage in decarbonizing the electricity sector, Applied Energy 175 (2016) 368–379. URL: https://www.sciencedirect.com/science/article/pii/S0306261916305967. doi:https://doi.org/10.1016/j.apenergy.2016.05.014.

[35] M. Arbabzadeh, R. Sioshansi, J. Johnson, G. Keoleian, The role of energy storage in deep decarbonization of electricity production, Nature Energy (2019).

[36] D. S. Mallapragada, N. A. Sepulveda, J. D. Jenkins, Long-run system value of battery energy storage in future grids with increasing wind and solar generation, Applied Energy 275 (2020) 115390. URL: https://www.sciencedirect.com/science/article/pii/S0306261920309028. doi:https://doi.org/10.1016/j.apenergy.2020.115390.

[37] T. Latimer, P. Meier, Use of the experience curve to understand economics for at-scale egs projects, in: Proceedings of the 42nd Workshop on Geothermal Reservoir Engineering, Stanford, CA, 2017.

[38] A. Gringarten, P. Witherspoon, Y. Ohnishi, Theory of heat extraction from fractured hot dry rock, Journal of Geophysical Research 80 (1975) 1120–1124.

[39] J. Olson, C. Augustine, A. Eustes, W. Fleckenstein, Design considerations for applying multi-zonal isolation techniques in horizontal wells in a geothermal setting, in: Proceedings of the 40th Workshop on Geothermal Reservoir Engineering, Stanford, CA, 2015.

[40] T. Li, S. Shiozawa, M. W. McClure, Thermal breakthrough calculations to optimize design of a multiple-stage enhanced geothermal system, Geothermics 64 (2016) 455–465. URL: https://www.sciencedirect.com/science/article/pii/S0375650516300712. doi:https://doi.org/10.1016/j.geothermics.2016.06.015.

[41] M. McClure, C. Kang, A three-dimensional reservoir, wellbore, and hydraulic fracturing simulator that is compositional and thermal, tracks proppant and water solute transport, includes non-darcy and non-newtonian flow, and handles fracture closure, in: Presented at the SPE Reservoir Simulation Conference, Montgomery, TX, 2017.

[42] M. McClure, C. Kang, C. Hewson, S. Medam, ResFrac Technical Writeup, Technical Report, ResFrac Corporation, Palo Alto, CA, 2021. Accessed July 27, 2021: https://www.resfrac.com/wp-content/uploads/2021/06/ResFrac-Technical-Writeup-February-13-2021.pdf.

[43] D. Hu, Y. Zheng, Y. Wu, S. Li, Y. Dai, Off-design performance comparison of an organic rankine cycle under different control strategies, Applied Energy 156 (2015) 268–279. URL: https://www.sciencedirect.com/science/article/pii/S0306261915008582. doi:https://doi.org/10.1016/j.apenergy.2015.07.029.

[44] Caiso oasis, http://oasis.caiso.com/mrioasis/logon.do, 2021. Accessed: 2021-04-8.

[45] Ercot market prices, http://www.ercot.com/mktinfo/prices, 2021. Accessed: 2021-03-24.

[46] J. Jenkins, N. Sepulveda, Enhanced Decision Support for a Changing Electricity Landscape: The GenX Configurable Electricity Resource Capacity Expansion Model, Working Paper, MIT Energy Initiative, Cambridge, MA, 2017.

[47] D. Lew, G. Brinkman, E. Ibanez, A. Florita, M. Heany, B.-M. Hodge, M. Hummon, G. Stark, J. King, S. Lefton, N. Kumar, D. Agan, G. Jordan, S. Venkataraman, The Western Wind and Solar Integration Study Phase 2, Technical Report NREL/TP-5500-55588, National Renewable Energy Laboratory (NREL), Golden, CO, 2013.

[48] E. L. Majer, R. Baria, M. Stark, S. Oates, J. Bommer, B. Smith, H. Asanuma, Induced seismicity associated with enhanced geothermal systems, Geothermics 36 (2007) 185–222. URL: https://www.sciencedirect.com/science/article/pii/S0375650507000387. doi:https://doi.org/10.1016/j.geothermics.2007.03.003.

[49] N. Sepulveda, J. Jenkins, A. Edington, D. S. Mallapragada, R. Lester, The design space for long-duration energy storage in decarbonized power systems, Nature Energy (2021).

[50] B. Adams, J. Ogland-Hand, J. M. Bielicki, P. Schädle, M. Saar, ChemRxiv, 2021. Preprint, DOI: 10.26434/chemrxiv.13514440.v1.

[51] G. Mines, GETEM User Manual, Technical Report INL/EXT-16-38751, Idaho National Laboratories, Idaho Falls, ID, 2016. Accessed May 5, 2021: https://workingincaes.inl.gov/SiteAssets/CAES%20Files/FORGE/inl_ext-16-38751%20GETEM%20User%20 Manual%20Final.pdf.

[52] S. Akar, C. Augustine, P. Kurup, M. Mann, Global value chain and manufacturing analysis on geothermal power plant turbines, in: Presented at the 41st Geothermal Resource Council Annual Meeting, Salt Lake City, UT, 2017.

[53] NREL (National Renewable Energy Laboratory), 2020 Annual Technology Baseline, Technical Report, National Renewable Energy Laboratory, Golden, CO, 2020.

[54] B. Barker, A. Pingol, Geysers reservoir performance - an update, in: Proceedings of the Twenty-Second Workshop on Geothermal Reservoir engineering, Stanford, CA, 1997.

[55] R. Freeze, J. Cherry, Groundwater, Prentice-Hall, Englewood Cliffs, N.J. U.S.A., 1979.

[56] T. Reilly, O. Franke, G. Bennett, The Principle of Superposition and its Application In Ground-Water Hydraulics, Technical Report OFR 84-459, U.S. Geological Survey, Albuquerque, NM, 1984.

[57] B. M. Adams, P. Schädle, genGEO: coupled reservoir-electricity-cost geothermal simulator, 2020. URL: `https://doi.org/10.5281/zenodo.4383139`. doi:10.5281/zenodo.4383139.

[58] W. Gorman, A. Mills, R. Wiser, Improving estimates of transmission capital costs for utility-scale wind and solar projects to inform renewable energy policy, Energy Policy 135 (2019) 110994. URL:

https://www.sciencedirect.com/science/article/pii/S0301421519305816.
doi:https://doi.org/10.1016/j.enpol.2019.110994.